DORBATH

Geometry, segmentation and stress regime of the Spitak (Armenia) earthquake from the analysis of the aftershock sequence

L. Dorbath,[1,2] C. Dorbath,[1,2] L. Rivera,[1] A. Fuenzalida,[1] A. Cisternas,[1] R. Tatevossian,[3] J. Aptekman[3] and S. Arefiev[3]

[1] *Institut de Physique du Globe de Strasbourg, 5 Rue René Descartes, 67084 Strasbourg Cedex, France*
[2] *ORSTOM, 213 rue La Fayette, 75480 Paris Cedex 10, France*
[3] *Institute of Physics of the Earth, Soviet Academy of Sciences, Bolshaya Gruzinskaya 10, Moscow 123242, USSR*

SUMMARY

The aftershock sequence of the Spitak earthquake, as recorded by a dense portable network deployed around the source region, is analysed in order to obtain a precise description of the mechanics of the rupture. A collection of 708 well-recorded events corresponding to a period of about two weeks is studied, their hypocentres are accurately located, and their focal mechanisms are calculated individually as well as by a joint procedure that permits us to estimate the stress regime.

The epicentral distribution of these aftershocks indicates that the fault at depth extends well beyond the surface rupture towards the west and northwest. Neotectonic and seismic observations permit us to identify five segments broken during the earthquake. The southeastern one, oriented N140°, corresponds to the surface ruptures along the Alavar right lateral shear fault. The main surface ruptures, between Spitak and Gekhasar, correlate well with aftershocks showing a N120° trending fault surface, dipping 50° to the NE and acting as a thrust with a right lateral component. Two similar segments towards the west, are offset and hidden under active folds. A fifth segment, towards the NW, corresponds to a right lateral blind shear fault buried in depth, in the vicinity of the large Pambak–Sevan fault. 14 vertical sections across the fault, including focal mechanisms, illustrate these features.

A relocation of the main shock and aftershocks for the period before the installation of the portable network, confirms the spatial extent of the seismicity. The foreshock, the main shock and the strongest aftershock (4 min 20 s after the main shock) have approximately the same epicentre. Thus the rupture started at the crossing of the Pambak–Sevan and Alavar faults and propagated bilateraly from there, although the seismic moment associated to the Alavar branch is only about one sixth of the total moment.

The stress regime is one of triaxial compression with a σ_1 axis oriented N344°. The same orientation is given by the microtectonic observations made on the central segment of the surface ruptures, a result that agrees with previous estimates for the Georgian Caucasus.

Key words: aftershock, Armenia, earthquake, stress.

INTRODUCTION

The Armenian earthquake of 1988 December 7 (40.987°N, 44.185°E, 5 km depth, origin time: 07:41:24.2 UTM, $M_S = 6.9$ after NEIC) produced widespread destruction in the region around the cities of Spitak, Leninakan and Kirovakan. This region, located within the Lesser Caucasus, is of particular interest because it represents an early stage of continent–continent collision (Philip *et al.* 1989). At the same time, the joint occurrence of impressive surface faulting and intense aftershock activity, constituted a natural laboratory to study reverse faulting in a tectonic

environment different from that of the San Fernando (1971), the El Asnam (1980), the Coalinga (1983) or the Whittier Narrows (1987) earthquakes. The study following the event, included teleseismic and near-field seismic observations, neotectonics, geodesy, levelling, palaeoseismicity, radon content and other physical observations.

12 days after the earthquake, a French–Soviet seismic network was installed in the epicentral area, and preliminary results from this expedition have been published elsewhere (Cisternas *et al.* 1989; Dufumier 1989; Jimenez, Cara & Rouland 1989). Another field team from the USA also obtained similar results (Pacheco *et al.* 1989). The portable networks complemented the near-source coverage of the permanent regional network of 27 Armenian, Georgian and Azerbaydzhan stations, some of which were damaged and failed to operate.

The field work experiment can be divided into three periods:

(1) from December 19 to December 24 the portable network was deployed and adjusted to provide the best possible coverage of the aftershock zone;

(2) from December 24 to January 8 the portable network of 26 sites distributed over an area of 1500 km^2 operated continuously;

(3) from January 8 to the end of February seismic monitoring continued but with a reduced network (20 sites).

The present paper discusses the aftershock distribution and focal mechanisms, the estimation of the stress regime and the construction of a detailed and accurate source model, from data obtained during the second period, when the information was of the best quality.

INSTRUMENTATION

The network, during the period under consideration, consisted of three different types of recorders (Fig. 1 and Table 1).

1 Analogue seismographs

10 of the sites were equipped with smoked paper recording seismographs (Sprengnether MEQ 800) and one component

Table 1. Temporary network.

Code	Name	Latitude	Longitude	Elevation	Type
AID	Aiderly	40° 46.70N	44° 22.80E	1550	D
COL	Col Krashen	40° 52.80N	43° 57.90E	1720	A
DAR	Darpas	40° 51.10N	44° 25.80E	1655	T
GOG	Gogaran	40° 54.10N	44° 11.70E	1900	T
KAP	Kaps	40° 52.30N	43° 45.20E	1700	D
KAT	Katnakhpior	41° 01.10N	44° 11.10E	1750	D
KET	Keti	40° 52.70N	43° 51.00E	1730	D
KIR	Kirovakan	40° 47.20N	44° 29.50E	1525	A
KML	Chigdamal	40° 52.60N	44° 15.80E	1820	A
KM2	Chigdamal2	40° 53.30N	44° 16.75E	1900	T
KYB	Kuibishev	40° 58.40N	44° 15.90E	1596	A
LER	Lernavan	40° 46.70N	44° 09.10E	2020	T
LRN	Lemansk	40° 46.80N	44° 16.00E	1940	T
LYE	Lernapar	40° 44.80N	44° 09.80E	2150	A
MET	Metsparni	40° 52.60N	44° 07.60E	2200	T
MOL	Molakishlag	40° 44.20N	44° 25.00E	1880	A
NB2	Nalband	40° 48.90N	44° 10.30E	1740	A
SAR	Saral	40° 50.80N	44° 20.90E	1640	T
SAT	Sarapat	40° 56.60N	44° 03.00E	2100	T
SPZ	Spitak	40° 49.90N	44° 15.70E	1700	T
SRR	Saraart	40° 52.10N	44° 13.30E	1680	D
ST1	Stepanavan1	40° 59.90N	44° 23.90E	1405	D
ST2	Stepanavan2	41° 01.30N	44° 15.60E	1640	A
TOR	Torosgiukh	40° 56.10N	43° 52.40E	1980	D
TUN	Tunnel	40° 55.40N	44° 26.80E	1900	A
XYB	Khinkoyan	40° 50.10N	44° 01.20E	1920	A

vertical sensors (Mark Product L4C, $T_0 = 1$ s). The gains were set at 66, 72 or 78 dB according to the background noise, and the filters were set at the position 'out' for the low-pass, and at 30 Hz for the high-pass. At some places, the gains were temporary reduced during windy conditions. All of the instruments functioned at a speed of 60 mm per minute with a separation of 1 mm between consecutive traces, allowing for 48 hr of continuous operation. The seismographs included temperature compensated crystal clocks whose drifts were measured by comparing every two days (and simultaneously recording) the internal time signal with the reference time radio-transmitted by Moscow (14 994 kHz). Despite the severe temperature conditions, the clocks did not drift more than 0.05 seconds per day. Internal time marks were placed at the second thus permitting a reading precision of 0.05 s for *P*-waves.

2 Digital recording systems

Six Geostras digital recorders built at the Institut de Physique du Globe de Strasbourg were used to record signals from three-component seismometers (Mark Product
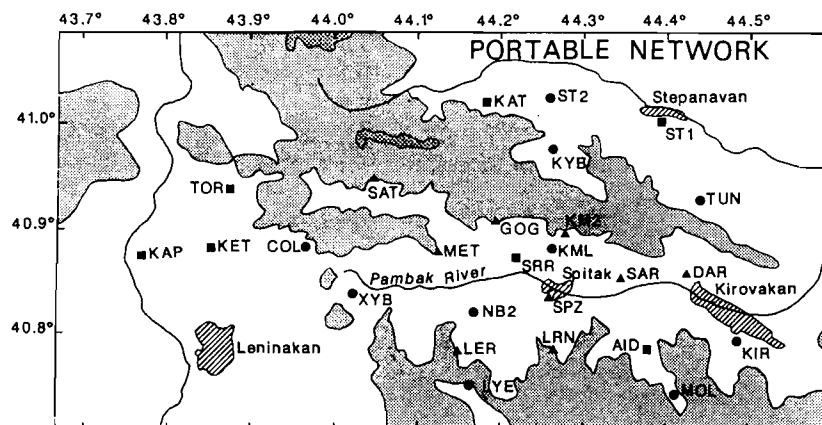

Figure 1. Locations of the temporary portable stations in the Spitak earthquake region (Table 1). Triangles: telemetric array. Circles: analogue stations. Squares: digital stations. The shaded contours are those of 2000 and 4000 m.

L22, 0.5 s natural period). The sampling rate was fixed at 150 samples per second. The recording process was triggered by a STA/LTA type algorithm, with the amplification being set automatically. Because of the limited dynamic range of the system (110 dB) some of the records of the strongest aftershocks were clipped.

Time signals were obtained from the worldwide Omega system. At some sites the drift of the receiving unit (Omegarec) crystal due to the very low temperatures (down to minus 20 °C) was faster than the built-in compensation process designed to correct the phase difference with respect to the incoming Omega signal. In these cases, the drift might have reached several seconds per day and absolute time is not available.

3 Telemetric network

Eight sites were equipped with a vertical component velocity transducer L4C, whose signals were transmitted via FM radio link to a central receiving station, where an additional three-component seismometer L22 was operating. The seismic signals together with the internal clock and the reference DCF time signals were digitized at a rate of 150 samples per second, mixed and then recorded on magnetic tape. The system is essentially the same as that of the autonomous Geostras stations. In this case, however, the recording process was activated only when any four of the stations jointly received a signal greater than a selected threshold within a given time period, to reduce the non-seismic triggering that occurs sometimes with the autonomous stations.

The locations of the telemetric stations were prescribed by the topography since they have to be within direct sight of the central station. The Spitak television tower was selected as receiving centre, so that the telemetric stations made up the kernel of the temporary network. Tapes were played back, arrival times of P- and S-waves were read and aftershocks automatically located every day. A subset of the hypocentre determinations thus obtained on a routine basis has been published in a previous paper (Cisternas *et al.* 1989). This knowledge of the aftershock distribution was very useful in selecting the sites of the autonomous stations to provide a uniform coverage in order to optimize hypocentral locations and constrain focal mechanisms. Except for the northwestern region to the north of the station SAT (Fig. 1), where the only existing road had been closed and access was impossible, the portable network of stations covers the aftershock area well.

DATA ANALYSIS

In the first days we recorded about 200 aftershocks per day with magnitude greater than 0.5 at the analogue stations; this number decreased slightly during the time interval of the present study (December 24 to January 8), staying nevertheless over a hundred by the end of the recording period. We studied only those events recorded at least by the telemetric network, though keeping in mind that this set of aftershocks is not really complete mainly due to short operational cut-offs and to difficulties in receiving the DCF time signals. We could have supplemented the gaps with events recorded only by the autonomous analogue stations

and by Geostras, however we preferred to maintain the homogeneity of quality for the data and results since, as we have said, the telemetric network was the essential part of our dispositive. About 750 aftershocks were thus located, 708 among which were selected on the basis of the quality of the solution.

1 Velocity model

First, we tried to find a reliable velocity model. For this purpose, and in order to ensure high-quality readings, we used data from the telemetric network. The V_P/V_S ratio was determined by using a composite Wadati diagram obtained from about one hundred aftershocks. We found this ratio to be 1.78. We checked that this value did not change significantly in the course of time, daily values ranging from 1.76 to 1.82.

With this V_P/V_S ratio of 1.78, we located about one hundred well-recorded aftershocks in a half-space with a P velocity ranging from 5.0 to 6.4 km s^{-1}. The minimum value of mean RMS was obtained for a velocity of 5.6 km s^{-1}. When we observed the minimum in the mean RMS as a function of hypocentral depth we realized that the P velocity increased with depth and then we chose a velocity model with two horizontal layers. Our best model was made of a thin layer of 4 km with a velocity $V_P = 5.3$ km s^{-1}, over a half-space with $V_P = 6.0$ km s^{-1}. The Soviet geophysicists exploded about 100 kg of TNT on January 23, in a drill-hole close to the epicentre of the main shock. This explosion was recorded by our network and analysis of the data confirmed that the upper crust velocity is about 5.3 to 5.4 km s^{-1}.

2 Hypocentre determinations

The aftershocks were determined by using the HYPOINVERSE program (Klein 1978) and good locations were selected on the basis of: RMS < 0.20 s and conditioning factor < 100. Some Geostras stations did not have correct absolute time for some periods as stated above, but we used $S-P$ times as data in those cases. Most of the locations rely on several S readings. The RMS is lower than 0.12 s for most of the locations (87 per cent), and 70 per cent correspond to conditioning factors less than 30 (Fig. 2), while 80 per cent of the aftershocks have standard errors on epicentral
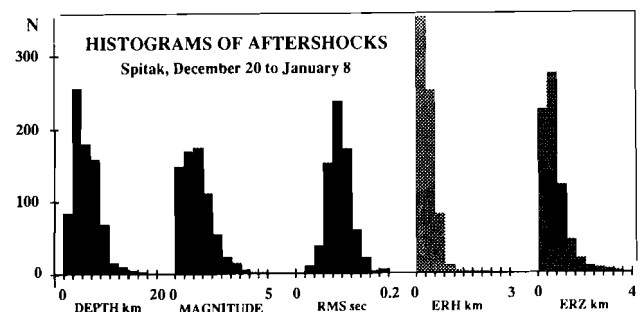

Figure 2. Histograms of (a) depth, (b) magnitude, (c) arrival time mean error, RMS, (d) epicentral error, ERH and (e) depth error, ERZ for the 708 selected events (1988 December 20 to 1989 January 8) (Klein 1978).

position and depth lower than 0.5 and 1 km respectively (Fig. 2). The latter values are known to be underestimates of the errors; however, when taken together with the RMS and the conditioning factor, they provide a reliable estimate of the quality of the locations. We located the whole set of aftershocks both, in a half-space model ($V_P = 5.6$ km s^{-1}), and in the selected two-layer model. The results do not differ significantly, as previously observed (Lyon Caen *et al.* 1988) when a network is dense and adequately covers the seismic zone; depths are tightly constrained by nearby stations. The epicentres differ by no more than 200 m on the average, and 83 per cent change by less than 500 m. The depths, which are more sensitive to model perturbations, differ by about 700 m on the average, 70 per cent of them changing by less than 1 km. Hence, we believe that the standard errors given by HYPOINVERSE are quite realistic.

3 Focal mechanisms

The polarity of each seismograph system was checked before the departure to Armenia, in the field by the recording of an explosion, and checked again upon the return to Strasbourg. Using a half-space model all the rays are direct ones, namely they have take-off angles greater than 90°. On the other hand, rays coming from hypocentres within the upper layer of a two-layer model, and diffracted at the lower interface, may hit a station as first arrivals. It follows that incidence angles, and therefore the distribution of polarities on the focal sphere, may change significantly. For these shallow events, we kept only those focal solutions for which the nodal planes did not vary much in azimuth and dip, when passing from the half-space to the two-layer model.

In this way, we have constructed individual fault-plane solutions for events with more than 10 P-wave polarities. The data set is of excellent quality and we could determine 412 focal solutions without contradictory polarities, and with an average of 14 readings. Nodal planes fitted by eye and maximum likelihood solutions (Udías *et al.* 1982) are in good agreement, and the nodal planes appear well constrained. Only a subset of these mechanisms is plotted on the cross-sections (Fig. 4), but all of them are to be considered in the section related to the fault mechanism. Table 2 shows the parameters defining nodal planes, azimuth, dip and rake, following Aki's convention (Aki & Richards 1980).

SPACE DISTRIBUTION OF AFTERSHOCKS AND FAULT-PLANE SOLUTIONS

The epicentres of the 708 well-located aftershocks are shown in Fig. 3. They depict a long (50 km) band, narrow in the eastern extremity, which widens to the west up to 10 km. The seismic activity appears to be weak in the upper 3 km. The hypocentres are superficial or shallow at the eastern end, but their depths increase to the west where they reach 14 km. It looks as if the relative amount of large magnitude aftershocks is higher at the western end, but this result may be due to the geometry and triggering system of the telemetric network. It seems convenient to define five main segments on the basis of the following seismological and tectonic considerations.

1 The Alavar southeastern segment

(Fig. 3; Fig. 4 AA', BB', CC', DD'; Table 2). The seismicity along this segment forms a very narrow zone, about 2 km wide and 15 km long, striking N140°. These general orientation and space distribution may be correlated to the Alavar fault (Philip *et al.* 1991), since the surface breaks pass through the epicentres at the southern tip, and they are slightly shifted west of the seismicity near the northern tip. Most of the shallow activity concentrates near the ends of this segment, seismicity at the centre being deeper. This distribution suggests that no further slip occurred on the area broken during the main shock, and that aftershock activity concentrated along the edges of the ruptured zone.

The seismicity seems to separate into two nearly vertical branches towards the southern edge of the segment and depths do not exceed 6 km (Fig. 4, a, b). Most of the focal mechanisms show stike–slip faulting on an almost vertical nodal plane striking at about the same direction as the general trend of the surface ruptures and the seismicity (N140°). Some reverse faulting occurs usually outside the main clusters.

Hypocentral depths increase up to 9 km towards the northern edge of the segment, the aftershocks lying on a single plane dipping about 65° to the northeast (Fig. 4CC', DD'). Cross-section CC' still shows dominant strike–slip faulting, however the relative amount of reverse faulting increases. The last cross-section (DD') suggests that the aftershocks define a clear fault plane. This cross-section, southeast of, but next to Spitak, is beyond the observed surface ruptures and shows as many strike–slip mechanisms as reverse ones, thus characterizing the transition to the next segment situated to the west of Spitak.

Hence, the Alavar segment exhibits shallow seismicity along a nearly vertical fault. The deformation is rather simple, most of the focal mechanisms being compatible with right lateral strike–slip faulting, if the nodal planes oriented along the general direction of the seismicity are selected as fault planes. This result is in agreement with the observation of surface ruptures which show oblique en échelon right lateral shears with a maximum displacement of 0.50 m (Philip *et al.* 1991). The seismic moment of this segment depends on the area of the broken surface (≈ 66 km^2) and on the relative offset across the fault (≈ 50 cm), and amounts to 1/6 of the total seismic moment released during the main shock (Haessler *et al.* 1991), and therefore much less important than the value given by Pacheco *et al.* (1989).

2 Central segments

(Fig. 3; Fig. 4, FF' to KK'; Table 2). The east central segment corresponds to the most important and continuous surface dislocations between Spitak and Gekhasar. These breaks extend for about 8 km (Fig. 3). They show reverse faulting dipping to the north with a right-lateral offset. The maximum vertical and lateral displacements were measured near Spitak: 160 and 40 cm respectively. On the other hand no surface breaks were observed along the western central segment where the fault is hidden under an anticline whose axis has about the same direction as the surface ruptures west of Spitak. This suggests that the rupture is hidden at depth, as indicated by the seismicity, and that the

Table 2. Aftershock parameters.

CROSS SECTION AA'

N	DATE	To	Latitude		Longitude		Depth	Mag	Strike	Dip	Strike	Dip	
1	890107	175712.2	40°	46.20	44°	22.81	3.45	2.6	268	50	43	50	1
2	890103	072026.9	40°	45.91	44°	22.48	3.16	2.7	281	69	33	51	2
3	881226	155420.8	40°	45.77	44°	22.25	3.30	1.5	117	80	216	72	3
4	890105	161449.8	40°	45.05	44°	22.68	3.65	0.7	312	80	42	70	4
5	890105	153026.4	40°	45.08	44°	22.74	3.77	2.5	304	70	43	73	5
6	890106	205323.0	40°	46.06	44°	22.16	3.91	2.7	311	61	53	75	6
7	881230	203557.4	40°	45.71	44°	22.46	4.03	1.2	330	60	65	80	7
8	881225	230724.8	40°	45.93	44°	22.03	4.61	1.9	310	54	209	84	8
9	890103	230330.5	40°	45.68	44°	22.00	5.34	1.6	330	60	83	55	9
10	890103	174712.4	40°	45.81	44°	21.93	5.46	1.1	326	70	64	60	10
11	881228	215607.5	40°	45.08	44°	22.78	8.49	1.0	321	62	216	72	11
12	890101	223846.9	40°	45.89	44°	23.22	4.32	1.2	290	70	192	70	12
13	881225	212250.9	40°	46.28	44°	23.34	4.25	1.9	291	72	33	61	13
14	890102	035014.4	40°	46.18	44°	23.33	4.16	1.8	253	71	148	60	14
15	881228	085132.9	40°	46.17	44°	23.47	5.46	1.6	297	82	36	70	15
16	881226	150430.5	40°	45.96	44°	23.82	4.78	1.9	318	80	60	62	16
17	890106	231443.1	40°	46.55	44°	23.37	4.10	2.8	318	78	57	66	17
18	890101	001023.3	40°	46.13	44°	23.88	4.01	2.0	305	50	88	51	18
19	881229	004237.1	40°	46.74	44°	23.70	4.32	1.3	122	75	17	53	19
20	881226	221126.0	40°	46.91	44°	25.56	4.73	2.3	263	50	92	40	20
21	881226	222756.8	40°	47.01	44°	25.42	4.05	1.7	266	62	7	79	21
22	890105	120225.3	40°	46.56	44°	23.05	3.48	2.1	102	87	192	79	22
23	890103	034014.1	40°	46.38	44°	23.25	3.43	1.9	128	78	226	74	23
24	890101	063129.3	40°	47.29	44°	25.01	2.92	2.3	120	60	232	45	24
25	890101	132048.0	40°	45.82	44°	24.14	2.52	1.5	260	50	108	44	25

CROSS SECTION BB'

N	DATE	To	Latitude		Longitude		Depth	Mag	Strike	Dip	Strike	Dip	
1	881226	82737.12	40°	47.06	44°	22.25	3.10	2.3	118	72	220	72	26
2	890107	144444.6	40°	47.44	44°	21.87	3.18	2.0	262	50	84	40	27
3	890101	124122.9	40°	46.91	44°	22.44	3.30	1.5	293	70	30	70	28
4	890106	184913.3	40°	46.72	44°	21.86	3.42	1.5	274	40	112	52	29
5	890106	230325.6	40°	46.16	44°	22.18	3.64	2.1	284	51	83	42	30
6	881228	202618.9	40°	45.72	44°	21.40	5.80	1.2	338	75	78	64	31
7	890107	075321.3	40°	47.11	44°	21.42	4.48	2.8	286	82	190	67	32
8	890107	030327.5	40°	47.11	44°	21.42	4.72	3.3	296	74	193	62	33
9	881229	002313.7	40°	46.11	44°	21.96	5.65	2.4	307	69	57	54	34
10	890104	185514.8	40°	47.05	44°	22.14	3.70	2.2	131	86	20	66	35
11	890104	024702.4	40°	47.17	44°	21.95	3.80	2.3	133	80	33	56	36
12	890107	150402.9	40°	47.37	44°	21.89	3.86	1.9	136	80	42	62	37
13	881226	033458.8	40°	47.12	44°	22.07	3.82	1.4	133	83	34	60	38
14	881226	113444.7	40°	46.72	44°	22.69	4.13	1.7	287	76	25	76	39
15	881227	120918.6	40°	46.92	44°	22.53	5.33	1.9	292	61	30	80	40
16	890105	214824.5	40°	47.05	44°	22.56	4.87	2.4	286	78	20	70	41
17	881227	000405.9	40°	46.64	44°	23.06	4.80	1.1	282	70	24	60	42
18	890104	223422.8	40°	47.37	44°	22.72	4.25	1.5	104	70	200	70	43
19	890104	140233.0	40°	47.39	44°	22.65	4.10	2.3	107	70	354	50	44
20	881227	031844.7	40°	46.71	44°	22.91	3.63	1.4	112	80	209	67	45
21	890101	231121.8	40°	46.97	44°	22.90	3.28	1.0	258	80	351	70	46
22	890101	225938.2	40°	46.76	44°	22.93	3.13	4.2	276	84	4	70	47
23	890105	025318.8	40°	46.98	44°	22.30	2.24	2.5	280	82	19	70	48

CROSS SECTION CC'

N	DATE	To	Latitude		Longitude		Depth	Mag	Strike	Dip	Strike	Dip	
1	890102	003002.2	40°	49.37	44°	19.34	3.40	1.6	250	60	70	30	49
2	890107	040030.0	40°	48.92	44°	19.88	3.51	1.1	330	80	62	70	50
3	881229	174327.2	40°	49.19	44°	19.20	3.73	1.9	333	80	64	70	51
4	890102	184737.2	40°	49.37	44°	19.07	4.80	0.7	321	70	57	70	52
5	881229	221000.3	40°	49.83	44°	18.75	4.66	1.3	345	89	180	2	53
6	890105	045923.9	40°	49.52	44°	19.28	5.57	1.2	317	86	56	40	54
7	890108	130138.3	40°	49.45	44°	19.20	5.64	3.5	311	67	53	72	55
8	890105	191703.1	40°	49.56	44°	19.14	5.99	3.0	324	57	72	68	56
9	890104	235619.2	40°	49.61	44°	19.21	6.21	3.4	312	68	54	73	57
10	890105	081513.6	40°	50.12	44°	19.17	6.46	4.2	287	61	27	81	58
11	890104	015404.9	40°	49.43	44°	20.43	6.86	1.7	294	30	70	68	59
12	890105	164824.8	40°	50.15	44°	19.19	7.24	0.8	238	46	95	50	60
13	881230	165916.2	40°	49.98	44°	19.40	8.18	1.0	131	83	34	77	61
14	890104	001804.4	40°	49.79	44°	20.14	5.98	1.2	238	60	358	50	62

Table 2. (*continued*)

CROSS SECTION CC'

N	DATE	To	Latitude		Longitude		Depth	Mag	Strike	Dip	Strike	Dip	
15	890107	150227.7	40°	50.38	44°	19.57	6.29	1.6	247	41	24	59	63
16	890102	203855.5	40°	49.76	44°	20.53	6.51	1.2	288	60	36	60	64
17	881231	194551.2	40°	50.14	44°	19.80	5.75	1.5	246	60	5	50	65
18	890101	091228.5	40°	50.38	44°	20.57	6.80	1.9	294	61	35	77	66
19	881229	170905.7	40°	49.87	44°	20.96	6.34	1.3	276	61	35	51	67
20	890107	175751.4	40°	49.88	44°	19.97	5.05	1.1	268	51	42	50	68
21	890101	005905.7	40°	49.52	44°	19.98	4.80	1.8	250	58	93	34	69
22	890102	234247.3	40°	51.95	44°	21.72	4.66	1.6	110	70	272	20	70
23	881230	161637.8	40°	49.46	44°	19.10	3.78	1.2	100	77	359	66	71
24	881230	050346.8	40°	49.67	44°	19.08	3.58	0.8	283	84	14	80	72
25	881230	050235.7	40°	49.57	44°	19.14	3.42	3.0	306	80	37	86	73

CROSS SECTION DD'

N	DATE	To	Latitude		Longitude		Depth	Mag	Strike	Dip	Strike	Dip	
1	881231	042655.2	40°	50.13	44°	17.37	3.12	2.0	300	62	42	80	74
2	881226	071439.9	40°	49.69	44°	18.14	3.23	1.1	330	69	80	54	75
3	881225	203533.8	40°	50.24	44°	17.67	3.91	0.7	352	74	88	75	76
4	890101	165116.2	40°	49.78	44°	18.28	4.05	1.1	292	60	34	70	77
5	881231	162619.9	40°	50.30	44°	18.74	4.95	1.6	288	50	24	80	78
6	881229	175938.6	40°	50.29	44°	19.19	6.04	1.5	284	49	34	71	79
7	890102	015004.1	40°	50.32	44°	19.19	6.07	0.6	318	40	214	80	80
8	890101	134025.6	40°	50.37	44°	19.15	6.16	0.9	278	37	22	80	81
9	881225	174943.9	40°	51.00	44°	17.96	6.83	1.5	232	62	51	28	82
10	881225	165117.6	40°	51.05	44°	18.05	6.85	1.6	252	76	19	26	83
11	881227	001503.6	40°	51.19	44°	18.00	6.97	1.8	255	64	55	28	84
12	890105	113058.1	40°	50.88	44°	18.25	7.77	1.7	96	60	208	61	85
13	890101	130211.4	40°	50.61	44°	18.93	7.60	1.7	270	61	49	38	86
14	881231	061526.8	40°	50.83	44°	17.87	12.52	0.9	308	70	62	40	87
15	890108	034339.7	40°	51.01	44°	18.65	8.47	1.9	295	80	40	40	88
16	890107	155058.9	40°	50.81	44°	18.84	7.27	1.1	256	35	76	55	89
17	890101	063510.5	40°	50.43	44°	19.30	6.45	2.6	296	65	41	67	90
18	881229	25751.39	40°	50.47	44°	19.36	6.27	2.2	246	61	358	61	91
19	881225	193617.2	40°	50.52	44°	19.42	6.47	1.4	232	60	48	30	92
20	890101	164744.7	40°	51.57	44°	19.83	7.65	1.2	264	50	104	42	93
21	890104	012708.3	40°	51.77	44°	19.48	7.50	1.5	327	70	69	60	94
22	881229	182512.8	40°	50.27	44°	19.11	5.82	1.0	275	80	22	46	95
23	881229	175542.9	40°	50.26	44°	19.16	5.75	1.1	304	27	189	81	96
24	890107	115555.2	40°	50.90	44°	17.74	4.09	1.8	298	40	149	54	97
25	890101	110202.3	40°	50.44	44°	18.26	3.44	1.0	265	36	108	56	98
26	881226	075210.2	40°	50.57	44°	17.44	3.56	1.6	209	46	41	45	99

CROSS SECTION EE'

N	DATE	To	Latitude		Longitude		Depth	Mag	Strike	Dip	Strike	Dip	
1	890104	170946.2	40°	51.10	44°	17.52	2.86	1.9	274	70	14	66	100
2	890104	185453.9	40°	51.44	44°	16.70	3.47	1.5	88	70	355	80	101
3	881229	101721.2	40°	50.96	44°	16.99	3.56	1.2	254	80	163	90	102
4	890104	232546.1	40°	51.05	44°	17.36	3.57	1.3	232	50	52	40	103
5	890103	165334.0	40°	51.46	44°	16.57	3.83	1.9	225	46	70	47	104
6	881227	041400.2	40°	50.99	44°	17.62	4.81	1.8	188	68	55	33	105
7	881228	180753.8	40°	51.65	44°	16.42	5.23	2.3	290	40	110	50	106
8	890101	050055.4	40°	51.59	44°	16.08	5.72	2.1	340	59	235	71	107
9	890102	080520.7	40°	51.31	44°	17.11	6.02	2.2	285	28	99	62	108
10	881226	145126.0	40°	52.29	44°	16.69	5.56	1.4	88	61	192	76	109
11	890104	233930.7	40°	50.92	44°	17.56	9.00	1.1	288	70	20	80	110
12	890102	205505.2	40°	50.78	44°	17.20	9.70	0.7	126	80	34	80	111
13	890103	185338.3	40°	51.67	44°	16.92	10.88	0.9	312	48	157	45	112
14	890101	144548.2	40°	51.95	44°	16.70	7.45	1.0	330	70	150	20	113
15	890104	060134.3	40°	52.33	44°	17.83	8.02	1.1	263	15	63	76	114
16	890101	094047.7	40°	53.24	44°	18.68	6.70	1.4	109	80	204	60	115
17	890102	211358.7	40°	53.80	44°	18.16	7.25	1.6	122	74	232	48	116
18	881225	220442.7	40°	53.79	44°	18.32	7.08	2.0	249	77	148	70	117
19	881231	153519.6	40°	52.98	44°	18.60	4.64	3.6	265	70	75	20	118
20	881231	191028.8	40°	52.94	44°	18.77	3.99	1.7	295	40	106	50	119
21	881229	005447.5	40°	53.19	44°	18.54	4.08	1.0	279	25	105	66	120
22	881231	102639.6	40°	53.13	44°	18.52	3.94	2.3	283	45	91	46	121
23	881231	174036.8	40°	52.92	44°	18.67	3.93	1.1	100	80	208	30	122
24	890105	195437.5	40°	52.91	44°	17.89	3.62	1.3	100	46	244	50	123

Table 2. (*continued*)

CROSS SECTION FF'

N	DATE	To	Latitude		Longitude		Depth	Mag	Strike	Dip	Strike	Dip	
1	881231	155434.1	40°	52.28	44°	15.71	3.43	4.2	222	36	59	56	124
2	881226	144303.3	40°	52.18	44°	15.43	3.38	2.7	289	70	28	82	125
3	890101	044235.9	40°	50.55	44°	14.33	3.23	0.8	298	80	28	84	126
4	881230	015330.9	40°	50.94	44°	14.04	3.34	1.3	94	90	184	70	127
5	881227	002609.9	40°	51.32	44°	14.88	3.85	0.9	289	83	35	83	128
6	881230	025318.7	40°	51.76	44°	15.30	4.43	2.0	332	62	227	68	129
7	890101	050055.4	40°	51.59	44°	16.08	5.72	2.1	340	59	235	71	130
8	881225	205758.3	40°	51.89	44°	15.76	6.98	2.4	310	34	115	57	131
9	890105	141522.7	40°	52.09	44°	15.85	6.83	1.2	270	50	111	42	132
10	890101	001521.7	40°	51.67	44°	16.04	7.87	1.1	338	56	158	34	133
11	890102	073722.8	40°	52.50	44°	15.81	6.31	1.5	265	40	85	50	134
12	881229	101506.1	40°	52.77	44°	15.09	7.54	0.5	323	61	84	51	135
13	881225	224127.1	40°	52.82	44°	15.00	8.27	1.5	290	69	42	50	136
14	890101	042011.3	40°	52.66	44°	15.67	6.93	0.7	324	50	144	40	137
15	890101	202929.0	40°	52.76	44°	15.79	6.45	1.5	265	50	85	40	138
16	890101	004901.6	40°	53.12	44°	15.40	6.81	1.2	288	40	108	50	139
17	890107	162442.9	40°	53.50	44°	16.30	5.26	1.1	95	85	186	80	140
18	890105	231830.2	40°	53.73	44°	17.22	5.95	1.2	292	71	36	71	141
19	890105	135457.4	40°	53.47	44°	15.52	3.67	2.7	246	35	69	56	142
20	890107	184907.4	40°	53.49	44°	15.51	3.98	2.7	220	40	62	53	143
21	880201	163319.2	40°	53.00	44°	17.07	4.16	3.3	316	70	185	30	144
22	881230	101559.1	40°	53.11	44°	16.77	3.93	1.5	92	72	194	69	145
23	881231	203301.5	40°	53.47	44°	16.37	3.48	1.6	281	36	104	54	146
24	890102	060359.4	40°	53.37	44°	17.25	3.38	1.3	240	40	74	50	147
25	890108	012844.0	40°	53.46	44°	16.66	3.20	1.2	112	79	270	10	148
26	890104	135842.9	40°	53.23	44°	15.96	3.59	2.2	308	68	203	62	149

CROSS SECTION GG'

N	DATE	To	Latitude		Longitude		Depth	Mag	Strike	Dip	Strike	Dip	
1	881226	154337.5	40°	52.32	44°	13.43	4.03	1.9	289	70	186	60	150
2	890102	011820.1	40°	51.70	44°	14.02	3.84	0.3	205	50	55	44	151
3	890108	052846.6	40°	52.14	44°	12.66	4.26	2.0	340	80	74	70	152
4	881225	215511.0	40°	51.79	44°	12.88	4.27	1.1	316	75	64	44	153
5	881225	163205.2	40°	52.03	44°	12.36	4.56	0.8	274	64	166	64	154
6	890108	090456.9	40°	51.93	44°	13.13	4.47	2.3	243	40	66	50	155
7	890103	134847.1	40°	52.06	44°	12.47	5.33	3.6	332	72	230	56	156
8	881226	025409.1	40°	51.89	44°	12.64	5.77	1.1	239	47	41	45	157
9	890103	081954.8	40°	52.17	44°	12.76	5.19	4.2	264	48	59	46	158
10	890103	083619.7	40°	52.31	44°	12.70	5.84	1.3	242	60	76	30	159
11	881231	142548.8	40°	52.96	44°	13.14	5.05	1.0	227	40	76	54	160
12	881226	175605.9	40°	52.83	44°	14.29	7.33	1.5	312	62	128	28	161
13	890103	213421.2	40°	53.02	44°	13.66	8.13	1.7	120	42	11	75	162
14	890107	142005.8	40°	53.04	44°	14.00	8.03	1.3	112	60	9	70	163
15	890106	235401.3	40°	53.22	44°	13.66	10.43	2.2	111	67	357	39	164
16	881229	094952.8	40°	53.40	44°	13.54	10.45	1.7	130	77	38	83	165
17	890103	175211.8	40°	53.35	44°	14.12	9.68	1.1	318	74	134	16	166
18	881230	052330.7	40°	53.40	44°	13.43	9.05	0.3	336	58	88	62	167
19	881229	144842.5	40°	53.34	44°	13.67	6.80	2.6	284	65	38	53	168
20	890108	113330.1	40°	53.40	44°	13.82	6.44	1.5	160	60	58	70	169
21	881230	190730.6	40°	53.42	44°	13.59	6.21	1.8	320	80	222	70	170
22	890102	223441.0	40°	53.19	44°	13.56	6.08	2.2	214	26	38	64	171
23	890102	020327.4	40°	54.09	44°	14.69	5.43	1.3	112	88	292	2	172
24	890104	072940.4	40°	53.32	44°	14.96	4.94	4.8	81	77	182	65	173
25	881229	100544.9	40°	53.19	44°	14.33	4.94	1.5	80	66	244	26	174

CROSS SECTION HH'

N	DATE	To	Latitude		Longitude		Depth	Mag	Strike	Dip	Strike	Dip	
1	881227	022319.8	40°	51.88	44°	11.73	3.90	0.6	286	40	109	50	175
2	890102	055608.7	40°	51.35	44°	11.35	4.37	0.7	252	63	104	30	176
3	881231	163003.7	40°	52.61	44°	11.92	4.96	0.8	214	50	101	64	177
4	890107	203718.0	40°	52.57	44°	12.53	5.82	1.7	255	50	75	40	178
5	881226	183007.1	40°	53.44	44°	12.22	6.40	2.3	219	62	85	39	179
6	890101	193649.5	40°	53.33	44°	12.58	6.43	1.4	235	40	91	57	180
7	881227	000622.1	40°	53.43	44°	11.99	6.67	1.7	294	51	46	69	181
8	881226	131103.0	40°	53.93	44°	11.99	6.37	1.7	295	72	34	80	182
9	881226	131124.3	40°	53.74	44°	12.08	6.44	2.6	295	50	39	80	183
10	881229	211619.8	40°	53.50	44°	12.82	6.86	0.9	255	28	130	75	184
11	890105	030755.1	40°	54.08	44°	11.78	7.00	1.4	254	40	66	50	185
12	890102	234639.1	40°	53.67	44°	12.68	7.13	1.2	204	50	21	40	186
13	881229	143210.8	40°	54.11	44°	11.99	7.70	3.0	235	54	66	37	187

Table 2. (*continued*)

CROSS SECTION HH'

N	DATE	To	Latitude		Longitude		Depth	Mag	Strike	Dip	Strike	Dip	
14	890102	014216.7	40°	54.05	44°	12.76	7.98	1.5	270	60	90	30	188
15	881230	023041.3	40°	54.08	44°	12.27	7.29	1.9	252	51	63	40	189
16	881229	220656.4	40°	54.08	44°	12.13	6.76	1.3	226	41	53	49	190
17	890102	145123.3	40°	53.54	44°	11.86	5.89	1.3	238	50	62	40	191
18	890103	170537.4	40°	53.33	44°	12.40	6.09	1.6	244	40	55	51	192
19	890107	023015.6	40°	53.29	44°	12.11	5.71	1.9	274	30	98	60	193
20	881229	112303.5	40°	53.49	44°	12.90	4.82	2.2	43	83	177	12	194
21	890103	012050.6	40°	52.91	44°	11.30	4.31	1.2	255	60	48	34	195

CROSS SECTION II'

N	DATE	To	Latitude		Longitude		Depth	Mag	Strike	Dip	Strike	Dip	
1	890105	043100.5	40°	53.48	44°	10.02	3.84	1.6	324	70	233	85	196
2	890102	095835.5	40°	52.52	44°	9.75	3.89	1.7	271	46	98	44	197
3	890101	132241.4	40°	52.78	44°	9.91	3.90	1.5	254	38	96	52	198
4	890107	043650.3	40°	53.50	44°	10.45	4.56	1.7	264	60	4	70	199
5	890105	170413.3	40°	53.70	44°	11.45	5.99	1.2	270	20	60	72	200
6	890106	095218.0	40°	54.46	44°	10.33	6.59	1.5	302	80	42	40	201
7	890105	201306.2	40°	54.08	44°	11.73	6.69	1.2	222	26	46	64	202
8	890103	232726.0	40°	54.29	44°	11.14	6.97	2.0	254	26	92	66	203
9	881230	064222.1	40°	54.68	44°	10.19	7.18	2.0	287	26	135	67	204
10	890101	170706.7	40°	54.06	44°	10.48	8.06	2.3	311	70	50	77	205
11	881230	153850.3	40°	54.32	44°	10.95	7.89	0.9	298	50	188	78	206
12	890105	160717.6	40°	54.10	44°	10.61	9.30	1.0	304	70	40	70	207
13	890105	202021.7	40°	54.25	44°	11.44	8.38	1.3	276	60	50	40	208
14	881226	072524.4	40°	54.41	44°	10.58	8.47	1.4	279	55	34	61	209
15	881230	054309.9	40°	54.39	44°	11.44	8.88	0.3	270	42	33	66	210
16	890101	154608.5	40°	54.78	44°	10.71	8.22	1.8	267	56	64	37	211
17	881229	214521.7	40°	54.63	44°	11.59	7.45	1.0	284	86	194	80	212
18	890107	115635.3	40°	54.75	44°	11.53	7.13	0.9	229	50	96	50	213
19	881227	013240.1	40°	55.00	44°	11.27	6.77	1.3	294	80	200	70	214
20	881230	124752.1	40°	54.97	44°	11.12	6.34	2.9	311	74	58	87	215
21	890101	173038.0	40°	54.15	44°	9.98	4.50	0.9	308	70	214	80	216
22	890108	064811.3	40°	53.86	44°	10.17	3.83	2.5	341	60	230	60	217
23	890102	042241.1	40°	53.97	44°	9.97	3.68	1.5	123	62	233	60	218
24	890105	162612.4	40°	53.73	44°	10.24	3.41	1.2	130	70	38	80	219

CROSS SECTION JJ'

N	DATE	To	Latitude		Longitude		Depth	Mag	Strike	Dip	Strike	Dip	
1	890105	140957.8	40°	53.99	44°	8.75	3.33	2.0	254	31	46	63	220
2	890102	185744.4	40°	53.84	44°	9.50	3.73	2.1	313	74	214	86	221
3	890103	144509.1	40°	53.64	44°	9.35	3.90	2.6	327	73	225	70	222
4	890102	083701.4	40°	53.10	44°	8.75	5.39	0.9	223	40	46	50	223
5	881231	045459.3	40°	54.89	44°	9.63	6.56	0.9	281	19	101	71	224
6	881228	234849.3	40°	55.21	44°	8.69	8.57	1.7	315	38	62	81	225
7	890107	005242.0	40°	54.25	44°	8.47	4.86	2.2	357	73	257	81	226
8	890108	102647.7	40°	54.18	44°	9.35	4.20	3.8	313	72	212	65	227
9	890105	142733.3	40°	54.34	44°	9.61	3.71	2.5	312	88	222	70	228
10	890101	020850.6	40°	54.04	44°	9.50	3.56	0.5	329	74	72	62	229
11	890105	223438.4	40°	54.17	44°	9.02	3.50	1.3	301	67	201	76	230

CROSS SECTION KK'

N	DATE	To	Latitude		Longitude		Depth	Mag	Strike	Dip	Strike	Dip	
1	881229	095238.4	40°	54.36	44°	7.25	3.79	2.2	323	79	74	87	231
2	881226	141244.0	40°	54.41	44°	6.41	3.68	2.1	315	83	61	83	232
3	890102	071647.6	40°	53.92	44°	5.94	3.45	1.7	280	35	104	55	233
4	881226	232132.9	40°	54.03	44°	6.38	3.99	1.8	285	81	25	73	234
5	881230	132251.6	40°	54.32	44°	6.94	4.56	1.2	327	82	65	82	235
6	890107	144651.5	40°	54.01	44°	5.91	4.50	2.3	273	50	65	44	236
7	890106	221618.9	40°	54.19	44°	7.52	4.97	1.7	301	55	56	61	237
8	881226	220310.6	40°	54.74	44°	6.50	5.37	0.7	257	40	142	74	238
9	890107	132509.8	40°	55.35	44°	8.16	7.33	1.8	281	40	65	57	239
10	890101	013132.6	40°	55.36	44°	7.94	8.25	0.9	285	51	80	43	240
11	881225	235736.3	40°	55.44	44°	8.65	7.64	0.8	320	40	77	71	241
12	881226	114550.2	40°	56.10	44°	7.90	10.30	1.80	286	50	109	40	242
13	890104	224525.4	40°	56.41	44°	8.13	9.85	2.2	292	88	22	75	243
14	890108	133241.0	40°	54.67	44°	7.14	4.44	2.2	303	59	41	82	244
15	881230	233004.0	40°	55.11	44°	8.20	3.65	1.9	328	68	78	57	245

Table 2. (*continued*)

CROSS SECTION KK'

N	DATE	To	Latitude		Longitude		Depth	Mag	Strike	Dip	Strike	Dip	
16	890108	142801.6	40°	55.58	44°	8.19	3.62	0.3	284	51	94	40	246
17	890105	185103.0	40°	59.89	44°	10.19	3.22	2.0	164	45	22	53	247
18	890106	192731.3	40°	55.01	44°	8.20	3.46	1.3	135	66	34	77	248
19	881226	153622.7	40°	54.71	44°	8.08	3.67	1.3	324	82	62	82	249

CROSS SECTION LL'

N	DATE	To	Latitude		Longitude		Depth	Mag	Strike	Dip	Strike	Dip	
1	890105	013646.2	40°	53.78	44°	5.26	3.93	1.4	275	80	174	40	250
2	890108	073151.0	40°	54.34	44°	4.31	5.36	2.6	302	50	78	50	251
3	890105	101039.9	40°	55.20	44°	5.32	6.88	1.4	324	84	56	80	252
4	881229	044245.8	40°	55.48	44°	4.78	6.98	1.9	290	31	68	66	253
5	890102	030406.5	40°	55.08	44°	5.62	7.01	2.0	292	28	34	84	254
6	881231	023047.1	40°	55.33	44°	5.15	7.44	1.6	289	41	51	67	255
7	881226	103526.2	40°	54.81	44°	4.58	9.79	1.7	283	70	22	77	256
8	881229	043543.4	40°	55.29	44°	4.74	9.76	1.1	279	60	118	32	257
9	881230	002208.7	40°	55.76	44°	6.04	12.64	2.5	272	50	148	59	258
10	881230	114617.1	40°	56.33	44°	6.31	11.35	0.7	280	60	100	30	259
11	881229	121613.6	40°	55.41	44°	6.24	8.11	1.5	276	76	14	76	260
12	890102	181108.8	40°	55.17	44°	5.99	6.57	1.9	103	80	212	30	261
13	890106	105053.1	40°	55.50	44°	5.83	6.27	1.4	308	50	45	80	262
14	890102	114809.7	40°	55.00	44°	5.72	5.87	0.8	270	56	54	40	263
15	890107	031117.5	40°	55.46	44°	5.19	5.49	1.0	310	60	50	70	264
16	881226	053057.4	40°	54.97	44°	5.62	5.50	1.6	300	56	32	84	265
17	881231	222356.9	41°	00.24	44°	8.71	3.60	2.1	168	84	71	71	266
18	881230	014615.1	40°	55.22	44°	6.22	3.45	2.5	304	71	45	79	267

CROSS SECTION MM'

N	DATE	To	Latitude		Longitude		Depth	Mag	Strike	Dip	Strike	Dip	
1	890104	053758.5	40°	55.02	44°	2.78	3.03	1.7	298	60	40	70	268
2	890103	142625.0	40°	54.63	44°	3.3	3.09	1.9	294	60	190	70	269
3	881229	72431.74	40°	54.93	44°	3.11	3.71	1.5	121	69	224	64	270
4	881226	103049.0	40°	54.41	44°	2.52	5.32	2.5	268	51	115	43	271
5	881227	021909.8	40°	55.57	44°	2.89	7.07	1.4	286	50	37	70	272
6	890103	074714.3	40°	55.19	44°	4.04	7.45	2.2	262	40	102	52	273
7	890101	091744.4	40°	53.96	44°	2.68	11.14	1.4	242	50	76	40	274
8	881231	115938.9	40°	53.84	44°	2.58	12.1	2.1	244	55	92	40	275
9	890102	145926.4	40°	56.97	44°	3.78	10.8	3.2	278	51	119	42	276
10	881229	222016.3	40°	55.76	44°	4.07	8.78	1.9	340	60	240	70	277
11	881229	141424.6	40°	55.82	44°	4.68	8.62	1.1	330	80	236	70	278
12	890107	145639.3	40°	55.62	44°	4.35	7.94	2.3	321	64	56	80	279
13	890102	002424.2	40°	55.8	44°	3.94	7.38	1.5	287	50	31	80	280
14	881225	155347.8	40°	58.1	44°	6.17	5.69	2.1	270	70	174	70	281
15	890108	061147.1	40°	58.12	44°	6.49	5.41	2.4	241	82	150	70	282
16	890101	223343.2	40°	55.44	44°	2.75	4.91	1.3	314	80	44	80	283
17	881227	020857.9	40°	55.18	44°	3.32	4.45	0.9	322	70	52	70	284

CROSS SECTION PP'

| N	DATE	To	Latitude		Longitude		Depth	Mag	Strike	Dip	Strike	Dip	
1	890107	131735.5	40°	53.91	43°	56.76	3.11	2.4	298	60	150	34	285
2	890105	004642.9	40°	52.37	43°	55.33	3.18	3.7	340	60	82	70	286
3	881231	214446.8	40°	55.67	43°	56.64	7.16	2.1	312	70	50	70	287
4	881227	010440.1	40°	55.34	43°	56.47	6.68	1.4	275	75	17	72	288
5	890104	172418.1	40°	54.33	43°	57.08	7.43	2.3	265	61	11	70	289
6	881231	041052.4	40°	55.02	43°	56.62	7.50	1.9	257	60	0	70	290
7	890102	010212.4	40°	54.74	43°	57.47	7.69	1.9	218	50	99	60	291
8	881231	060339.0	40°	54.28	43°	56.17	8.87	1.5	264	70	100	30	292
9	881231	143251.8	40°	54.87	43°	57.6	8.44	2.8	245	34	46	56	293
10	881230	133111.2	40°	54.74	43°	57.43	8.79	3.1	258	60	358	70	294
11	881230	165938.9	40°	54.91	43°	57.1	9.45	1.2	255	60	75	30	295
12	881231	040709.4	40°	55.13	43°	56.66	9.71	4.7	140	89	225	24	296
13	881229	184349.8	40°	55.63	43°	57.32	13.17	3.6	260	80	358	50	297
14	881231	052819.6	40°	54.92	43°	57.7	9.73	1.3	226	38	46	52	298
15	881231	101608.6	40°	55.13	43°	57.51	9.59	1.9	260	45	75	46	299
16	881231	045900.1	40°	55.37	43°	57.01	9.75	2	337	81	221	24	300
17	881229	140205.1	40°	55.06	43°	57.71	9.66	0.8	253	47	32	52	301
18	881226	200245.2	40°	57.84	43°	59	12.02	1	302	71	151	22	302
19	881226	184116.4	40°	55.23	43°	57.6	10.11	2.3	250	72	142	56	303
20	881231	043412.2	40°	55.28	43°	57.61	9.50	1.9	252	31	105	64	304
21	890108	000809.9	40°	56.4	43°	57.26	8.39	2	270	50	76	40	305
22	881230	024932.5	40°	59.38	44°	0.99	6.94	2.6	319	80	50	70	306
23	881228	224936.6	40°	58.99	44°	0.34	6.40	2.9	305	68	45	83	307
24	881228	224657.5	40°	58.86	44°	0.24	6.50	2.9	308	71	48	71	308
25	890101	221925.5	40°	59.17	43°	59.87	4.73	1.4	264	60	24	50	309
26	890101	094807.5	40°	59.21	44°	0.04	3.29	1.8	310	80	42	70	310
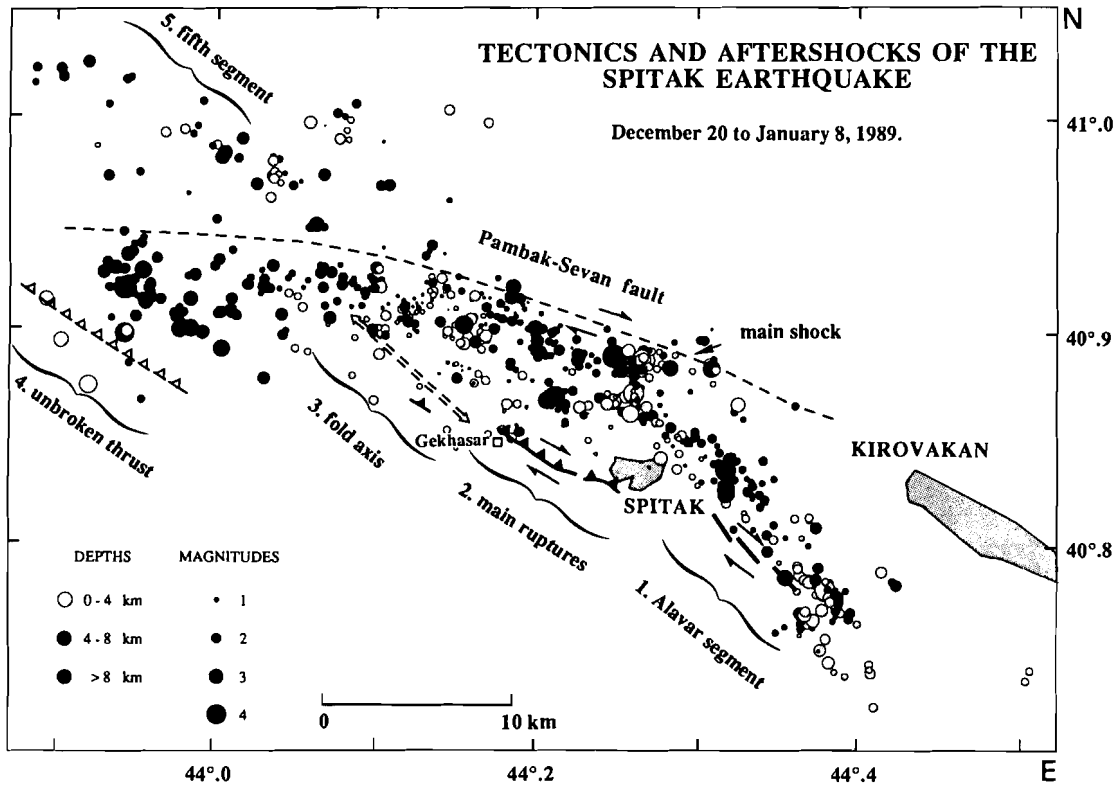
Figure 3. Map of the epicentres of the aftershocks from 1988 December 25 to 1989 Jaunary 8. The cross indicates our relocation of the epicentre of the main shock. Five distinct segments are shown. The main tectonic features are included: thicker lines show surface ruptures and the indentation shows the thrust dip, parallel segmented lines indicate the anticline axis, the indented segmented line is the unbroken thrust fault, the long broken line bordering the seismicity to the north is the Pambak–Sevan major fault.

deformation behaves in a plastic way at the surface (Stein & King 1984).

The aftershock distribution (Fig. 3) shows that the seismicity pattern changes abruptly to the west of Spitak: the azimuth shifts to N120°, the epicentre cluster widens, surface breaks are to the south of the epicentres, depths reach 10 km and more. Shallow activity is mainly concentrated near the edges of the surface breaks. Some of these near–surface events form elongated clusters transverse to the general direction of the seismicity (Fig. 4, FF' to KK') and might be related to transform faulting connecting adjoint segments. It is worth noticing that important shallow aftershocks take place just above the relocated hypocentre of the main shock (see below) and at the bend of the fault between the N120° and N140° oriented segments. Distribution of hypocentres with depth is not uniform (Fig. 3). The dip of the fault, about 55°, is in agreement with the GEOSCOPE average solution (Haessler *et al.* 1991). This dip, together with the greater depth of the hypocentres, explains the widening of the epicentral distribution with respect to the Alavar segment.

Fault-plane solutions in the transition regions between segments divide between strike–slip and reverse faulting, like those located on the main fault (Fig. 4 FF'). Cross-section HH', near the middle of the segment, shows a simple feature: hypocentres delineate a single fault plane and almost all focal mechanisms are reverse faulting (Fig. 4 HH'). Thus, mechanisms are dominantly reverse dip slip

in the central part, a right lateral component being frequent on the sides. Strike–slip faulting indicates left-lateral movement along the transverse lines of shallow seismicity which bound the segment at each end. The dominant feature of aftershock focal mechanisms, namely reverse faulting with pronounced right lateral component, is in fairly good agreement with the surface breaks.

We have to emphasize that while there are strong differences in the surface expression of the fault between the region Spitak–Gekhasar and the fold west of Nalband (Fig. 8), it is more difficult to resolve noticeable changes in the aftershock pattern near the transition.

3 Western segments

(Fig. 3; Fig. 4, MM', PP'; Table 2). West of the central segment the seismicity divides into two branches; one to the southwest and another one to the northwest.

Aftershocks extend over a zone approximately 10 km long with a general E–W elongation on the southwestern branch. The seismicity appears to be more scattered than along the previous segments, shallow activity is weak, and many aftershocks reach 15 km in depth. No surface ruptures have been observed along this segment. Although the general trend of the activity appears to be E–W on the map of epicentres, cross-sections with the same N30° azimuth as those of the central segment, exhibit a fairly well-defined plane (Fig. 4, PP'). Nevertheless, a geological fault
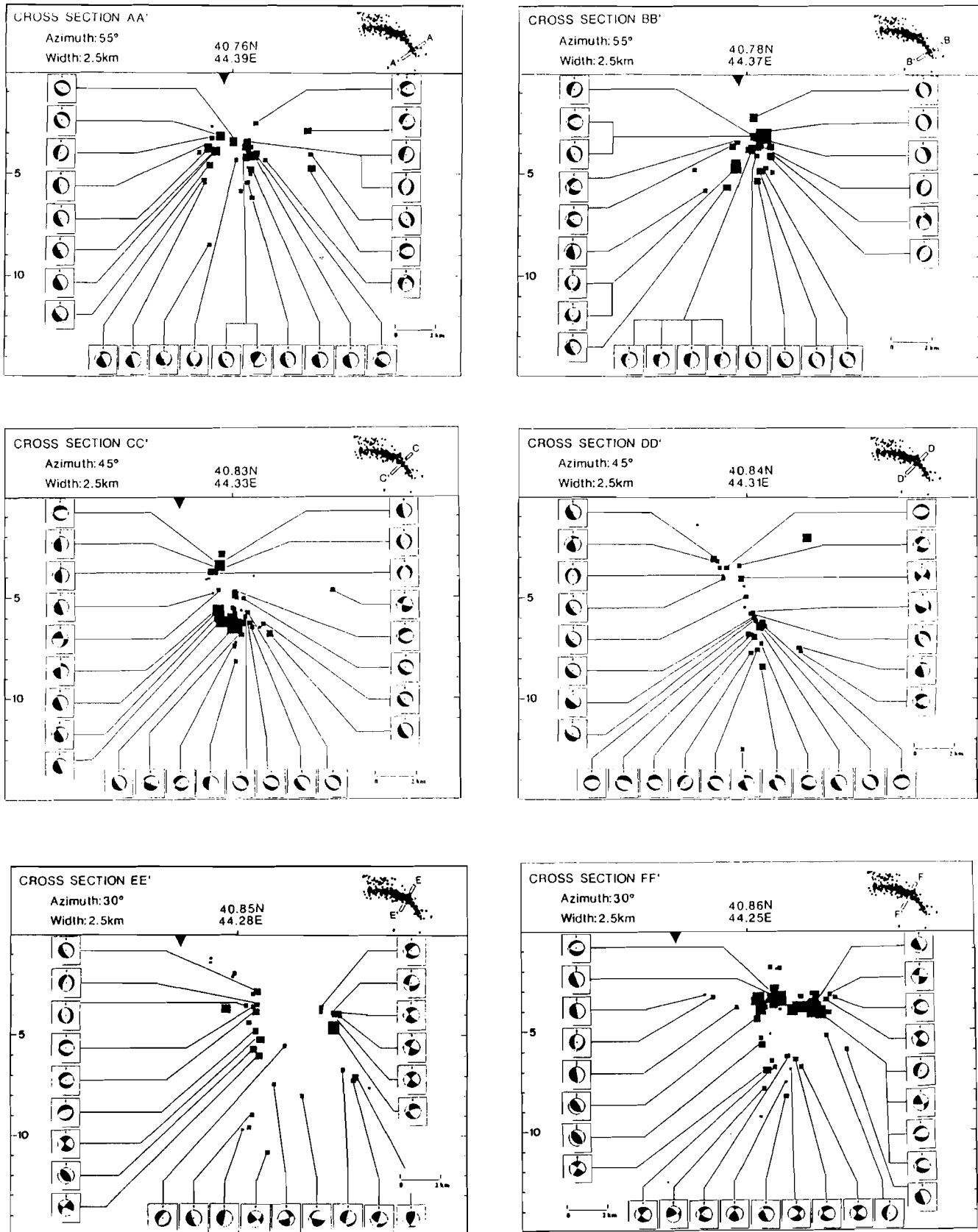
Figure 4. Cross-sections (AA' to PP') through the hypocentres of the aftershocks along the lines shown in the insets. No vertical exaggeration. Depth estimations have 1400 m above sea-level as reference level. The focal mechanisms are shown in the Schmidt equal area back projection roughly looking NW. An inverted triangle at the surface shows the trace of the fault, while the filled half circle indicates the position of an anticline. The coordinates of the central point of the section, its width and its azimuth are shown.
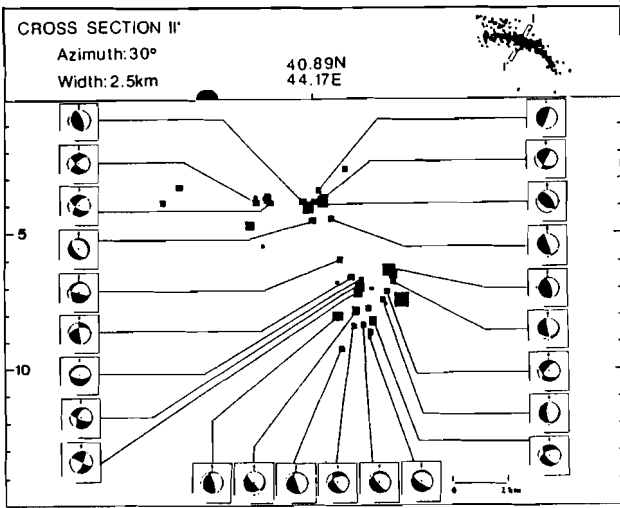
Figure 4. (*continued*)

CROSS SECTION MM'
Azimuth:30°
Width:2.5km
40.91N
44.05E

CROSS SECTION PP'
Azimuth:30°
Width:2.5km
40.95N
43.97E
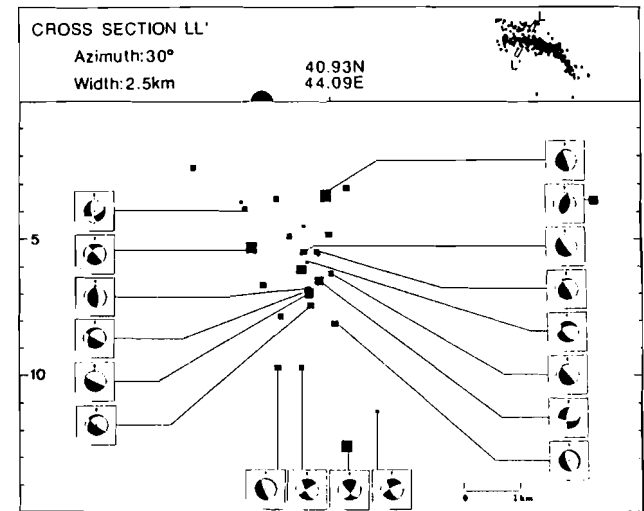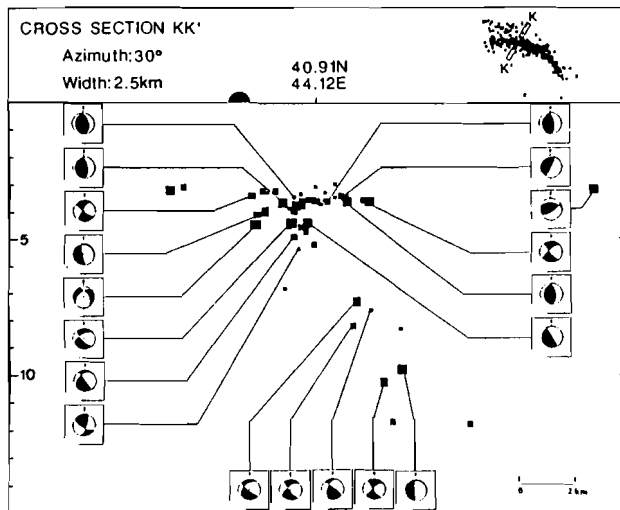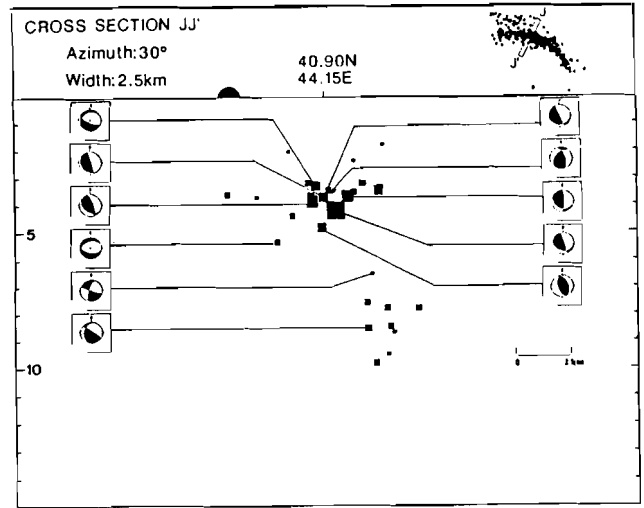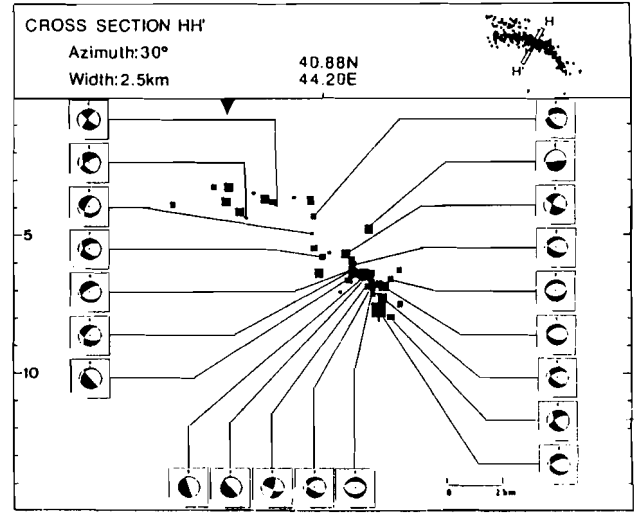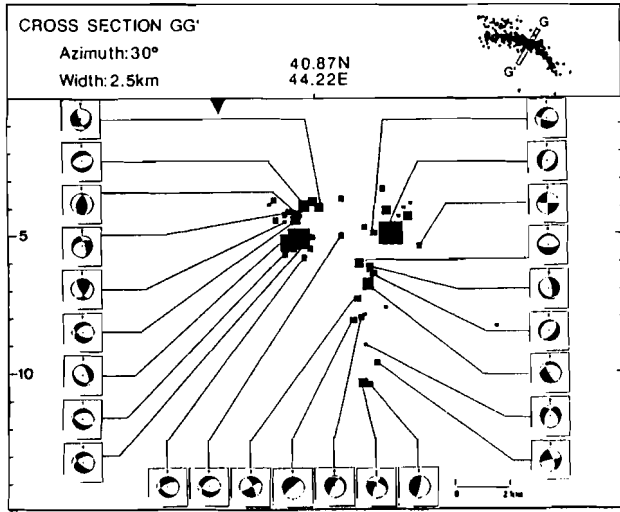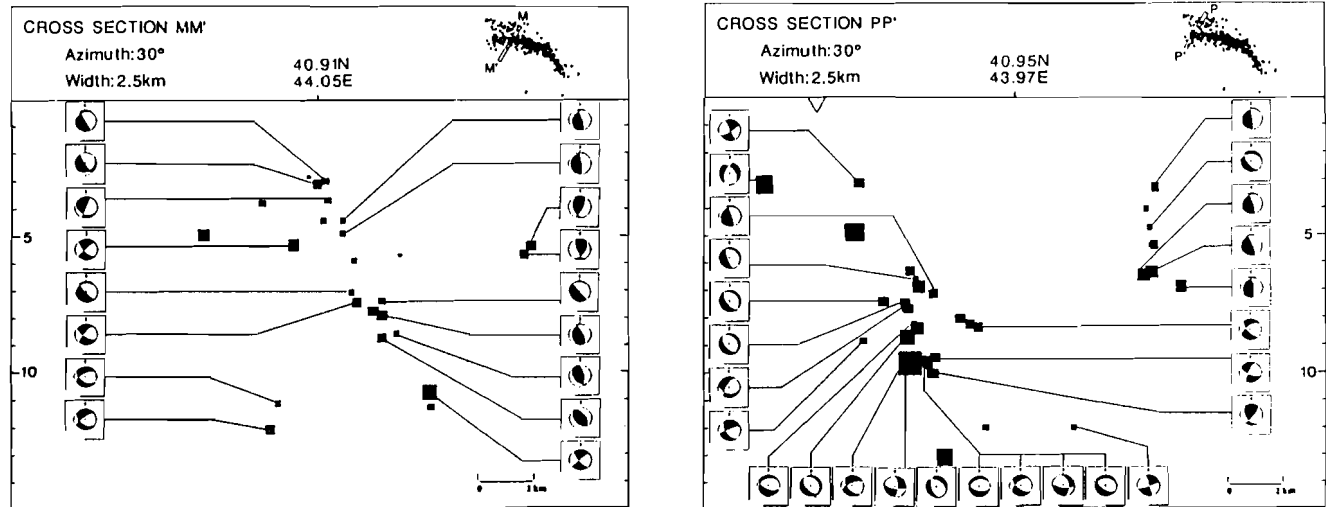
Figure 4. *(continued)*

apparently not active during the main shock borders the seismicity to the south, is well seen on satellite images, and was already known by the geologists before the earthquake. This fault, at least 10 km long and dipping to the north, has the same orientation as the surface breaks of the central segment, namely about N120°. From this evidence, we conclude that most of the seismic activity along the southwestern segment takes place on a fault plane parallel to the central segment fault plane and offset by about 4 km to the south; thus forming an 'en échelon' system. The dislocation did not reach the surface during the main shock. Focal mechanisms are comparable to those of the central segment, namely strike–slip faulting and reverse faulting, the latter being dominant.

The north western activity defines an elongated cluster of aftershocks (Fig. 3), whose depths range from 3 to more than 10 km. This branch is also prominent on cross-sections (Fig. 4 PP'), where it appears as a narrow vertical band. Practically all of the focal mechanicms in this segment are pure right lateral strike–slip.

Whereas all aftershocks clusters corresponding to the four previous segments end against the Pambak–Sevan fracture zone, which is the main tectonical feature of the area, this last branch extends beyond this structure. The depths vary from shallow to deep, and although several events have depths of less than 4 km, no surface breaks have been found in this northwestern region.

STRESS TENSOR AND FAULTING MECHANISM

The quality of the data gathered and the density of the network raised our expectations of mapping stress variations along the fault. The method developed by Rivera & Cisternas (1990) was used to determine the stress tensor. First we assumed that a unique stress tensor could explain the whole set of data, and performed the calculation using 155 aftershocks with more than 15 polarities. A normalized likelihood function of 97 per cent was obtained, and 94 per cent of the polarities were explained by a single tensor with

almost horizontal principal axes σ_y and σ_x (σ_z is the principal value with axis closer to the vertical, $\sigma_y > \sigma_x$, and the three are oriented to form a dextral reference frame) with strike N344° and N74° respectively, σ_z being nearly vertical (Fig. 5a, total data set), the shape factor, $R = (\sigma_z - \sigma_x)/(\sigma_y - \sigma_x) = -0.7$, being typical of a triaxial compression regime. This is a remarkable result that leaves very little room for variations of the stress.

Next, we determined a separate stress tensor for difference regions. The stress tensor corresponding to the southeastern segment is the same, but the uncertainty on the directions of σ_x and σ_y is large due to the lack of variety of the fault planes which are dominantly vertical and strike in the same direction. This is also why the shape factor is poorly resolved (Fig. 5b). The central segments offer more variety in azimuths and dips and the tensor is well constrained (Fig. 5c). The solution is the same as the one given by Philip *et al.* (1991) from striae measured on the exposed fault scarp between Spitak and Gekhasar. The same tensor is found again towards the west, but only the direction of σ_1 is well defined, since the shape factor is near zero indicating that $\sigma_z \approx \sigma_x$ and that the stress regime corresponds to uniaxial compression (Fig. 5d). The change is shape factor passing from the central ($R = -0.9$) to the western segment ($R = 0$) may be a real effect since the fault planes have different orientations and should contain the tensor well.

The major result is that the area where the earthquake occurred is subjected to a N344° compressive regime. A similar conclusion was obtained in the study of Philip *et al.* (1989) from microtectonic data collected in Georgia and at a much larger regional scale. However, these authors found that the minimum principal stress was horizontal and roughly oriented E–W. The reason for this difference is that they worked north of the Spitak area, in a region which contains NS oriented volcanic alignments and the corresponding normal faulting, among other tectonic features. This region, where EW extension is clear is connected to a similar one (also in EW extension) which is found at the southeast of Spitak, the Spitak fault acting as a transform
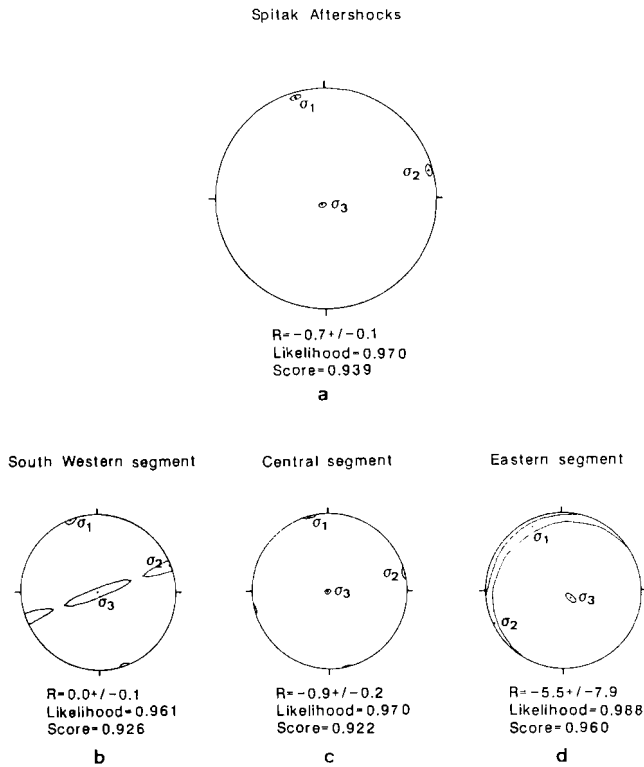
Spitak Aftershocks

R = -0.7 +/- 0.1
Likelihood = 0.970
Score = 0.939

a

South Western segment   Central segment   Eastern segment

R = 0.0 +/- 0.1   R = -0.9 +/- 0.2   R = -5.5 +/- 7.9
Likelihood = 0.961   Likelihood = 0.970   Likelihood = 0.988
Score = 0.926   Score = 0.922   Score = 0.960

b   c   d

Figure 5. Principal axes of the stress tensors in lower hemisphere Schmidt equal area projection. One standard deviation ellipses around the axes are shown. The shape factor $R = (\sigma_z - \sigma_x)/(\sigma_y - \sigma_x)$ indicates the stress regime (Rivera & Cisternas 1990). (a) Total data set of the aftershocks of Table 2. (b) South western segment. (c) Spitak–Gekhasar central segment. (d) Alavar eastern segment. Negative values of R corrrespond to triaxial compression, but the tensor has symmetries in cases (b), where two different faults are mixed, and (d) where we have almost one single fault plane.

fault between them (Philip *et al.* 1991). This explains the lack of normal faulting in the Spitak fault zone and the more compressive character of the resulting stress tensor.

Going back to the focal mechanisms of the aftershocks, the stress-tensor obtained from the whole set of data allows us to resolve some details related to the geometry and the process of faulting. A large number of focal mechanisms has been presented on the cross-sections, but the complete set will be used now. It is clear from the focal solutions shown earlier (Fig. 4) that the mechanisms range from strike–slip to pure reverse dip–slip. However, the rake is not evenly distributed, and a statistical study over the complete set shows that most of the mechanisms are either almost pure strike–slip (like in the sourtheastern segment), or nearly pure dip–slip (like in the central part of the central segment). More precisely, we divided the rake interval [0°, 90°] into four equal sectors and verified that 33 per cent of the mechanisms were almost pure strike–slip (rake within the [0°, 22.5°] interval), and 33 per cent almost pure dip–slip (rake within the [67.5°, 90°] interval).

In both cases, strike–slip faulting or reverse faulting, we chose as fault plane the one which was the closest to the general trend of seismic activity. Fig. 6 shows the histograms of the azimuths and dips of the chosen fault planes in polar

representation. A large majority of fault planes corresponding to strike–slip mechanisms have an azimuth range of 100°–150°, and dip steeper than 70°. A few of these aftershocks might actually have the other nodal plane as fault plane, as was suggested for the shallow alignments at the extremities of the central segment. On the other hand, dips are steeper than those of the planes observed on the cross-sections, except for the Alavar southeastern segment which shows complete agreement between the individual mechanisms and the fault plane obtained from the general trend of the seismicity. In addition to this we observe that the azimuth range for reverse mechanisms varies from 60° to 110°, this is about 40° less than the values obtained from the hypocentres for the general structural directions even though most dips range between 40° and 60°, namely about the same value as that defined by the cross-sections. These apparent discrepancies for the segments west of Spitak may be explained by the picture suggested by Scholz (1990, p. 27) and by King & Yielding (1984) where the ruptured surface is growing through a system of 'en échelon' smaller scale faults (aftershocks) along its rim, which are not on the same plane as the main fault.

The region experienced a long tectonic history (Philip *et al.* 1989) and the medium should be highly fractured. Then,

SPITAK: FOCAL MECHANISMS OF AFTERSHOCKS
DISTRIBUTION OF AZIMUTHS AND DIPS

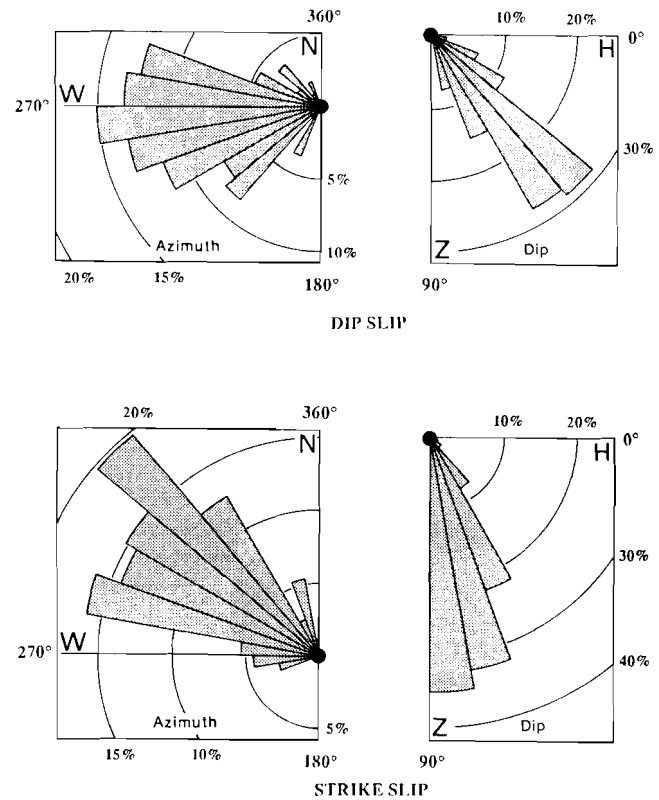DIP SLIP

STRIKE SLIP

Figure 6. Azimuths and dips of the fault planes for the 'reverse like' and 'strike–slip like' mechanisms of aftershocks respectively. The histograms are obtained after the sorting described in the text. Circles, in polar coordinates, indicate percentage of the total number of aftershocks. Azimuth varies between 180° and 360°, and dip between 0° and 90°, in steps of 10°.

under the actual stress regime, fracturing should occur along the most favourable surfaces: the pre-existing Alavar and Pambak–Sevan great faults (Philip *et al.* 1991). But as they intersect each other forming a sharp bend, it is likely that the Spitak–Gekhasar fault and the system of 'en échelon' blind folds that continues the deformation to the west, act in such a way as to smooth the transition from one fault to the other.

RELOCATION OF THE MAIN SHOCK AND EARLY AFTERSHOCKS

The epicentre of the main shock is 40.987°N, 44.185°E according to the National Earthquake Information Center (NEIC), 40.99°N, 44.25°E after the Euro-Mediterranean Seismological Center (EMSC) and 40.91°N, 44.25°E according to the seismological centre of Obninsk. Although these locations are close to each other, they differ by more than 10 km, and the uncertainty is too large to undertake detailed studies such as defining the sense of rupture, for example. In a similar way, location errors for the largest aftershocks that occurred on the days following the main shock, until the setting up of our temporary network, do not allow a detailed study of the evolution of the activity in space and time. In particular, the relation between the largest aftershock and the main shock is not clear on the basis of these locations.

Nevertheless, enough information was available from the local permanent networks to improve the epicentral determinations. We relocated the main shock and the principal aftershocks up to December 25 using two variants of the master event technique (Dewey 1972). The master events were strong aftershocks accurately located with the temporary network and for which we could say that we knew their absolute position with an accuracy of 0.5 km in epicentre and 1 km in focal depth. In the first technique, these master events were used to obtain station delays for the regional stations including Armenian, Georgian and Azerbaidjanian stations (Fig. 7). In the second variant, the main shock and early aftershocks were relocated relative to the master events by using an inversion algorithm (Tarantola & Valette 1982; Besse 1988).

To apply the first method we collected P arrival times from 23 regional stations ($\Delta < 350$ km) for 29 master events. S-wave station delays were obtained from P-waves delays simply by multiplying by 1.7. Data from stations ALG, ART and SHN were not available before 1988 December 11, when they were set up by the Moscow Institute of Physics of the Earth. Except for the nine Armenian stations with direct readings, all of the data was taken from bulletins. The data from the Stepanavan station (STE) were particularly useful because of its vicinity to the seismic zone, its continuous recording and the impulsive character of the onsets. After subtracting mean P- and S-wave station delays from the observed arrival times, we relocated the main shock and early aftershocks using the HYPOINVERSE program with a fixed focal depth (7 km).

In the second method, the data set consisted of P arrival times to nine of the Armenian stations read by one of us, plus P arrival times at three Georgian stations to the northwest of the area taken from bulletins after controlling their quality against our records of common events (Table 3, Fig. 7). The quality of the seismograms of Soviet stations is excellent and the service homogeneous. One minute of coded Moscow time is recorded once a day in the photographic traces of all stations, thus permitting a reading accuracy at least as good as a tenth of a second.
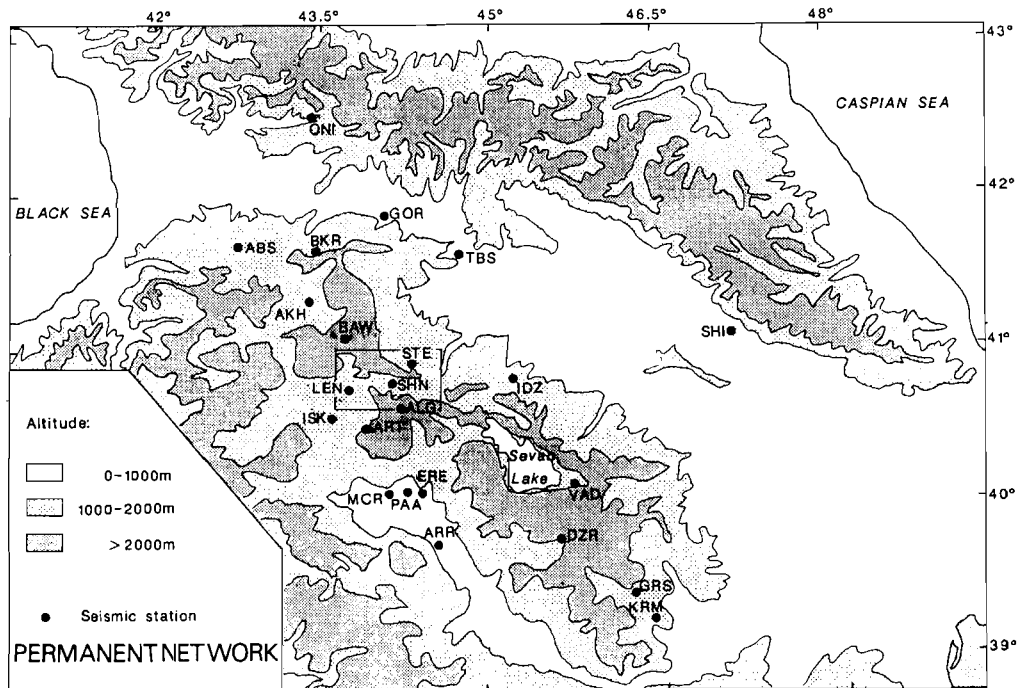

Figure 7. Topographical map of Caucasus with the sites of regional (Armenian, Georgian and Azerbaydzhanian) stations used for relocations. The rectangle shows the region surveyed by the portable network after the Spitak earthquake.

Table 3. Permanent stations. Asterisks denote Armenian stations.

Code	Name	Latitude	Longitude	Elevation
ABS *	Abastoumani	41° 45.00N	42° 49.00E	1700
AKH *	Akhalkalaki	41° 24.00N	43° 28.80E	1703
ALG	Alaguiaz	40° 40.80N	44° 17.20E	2010
ARR *	Ararat	39° 50.40N	44° 42.00E	850
ART	Artik	40° 34.40N	43° 59.90E	2280
BKR *	Bakouriani	41° 43.80N	43° 31.20E	829
ERE *	Erevan	40° 10.80N	44° 30.00E	1000
GOR	Gori	41° 59.00N	44° 08.00E	640
GRS	Goris	39° 31.20N	46° 19.80E	1398
IDZ *	Idjevan	40° 53.00N	45° 12.50E	1500
ISK *	Issaakian	40° 36.00N	43° 42.00E	1435
KRM	Karmrakar	39° 19.20N	46° 28.20E	1524
LEN *	Leninakan	40° 48.60N	43° 50.90E	1550
MCR *	Metsamor	40° 11.30N	44° 08.30E	850
ONI	Oni	42° 35.00N	43° 27.00E	810
PAA *	Parakar	40° 10.20N	44° 24.60E	810
SHI	Sheki	41° 13.00N	47° 12.00E	750
SHN	Shenavan	40° 51.60N	44° 13.20E	1400
STE *	Stepanavan	40° 59.90N	44° 23.90E	1390
TBS	Tbilissi	41° 44.00N	44° 45.00E	609
VAD *	Vardenis	40° 11.40N	45° 43.80E	1930

Six master events covering the aftershock area were selected. Each master event gave one hypocentre for each one of the aftershocks as output of the relative location routine. Out of the six hypocentres determined for each aftershock we kept the one with the minimum RMS value, checking that this solution was close to the hypocentre of the corresponding master event. The problem is almost one-dimensional due to the elongated shape of the aftershocks area and the two stations ISK and IDZ, respectively to the southwest and east of the seismic zone controlled the epicentral positions fairly well, when both P arrival times were available. Depths were poorly controlled and generally fixed to the depths of the master events.

About 80 aftershocks with magnitude greater than $M_L \approx 3.0$ were located using the second method (master events) (Table 4), but only half of this number by using station corrections, due to lack of data in the bulletins.

Table 4. Relocations.

1. **Relocation of the main shock with respect to the aftershock of 04-01-1989 at 07h 29mn**

Y M D	To	LAT N	LON W	DEPTH	RMS	ERX	ERY	ERZ	Mag
881207	7 41 24.61	40N53.14	44E15.65	5.46	.58	.22	.17	2.83	7.0

2. **Relocation of the foreshock with respect to the main shock**

Y M D	To	LAT N	LON W	DEPTH	RMS	ERX	ERY	ERZ	Mag
881206	15 27 7.80	40N49.41	44E11.83	5.46	.89	.15	.19	3.80	3.

3. **Relocation of the largest aftershock with respect to the main shock**

Y M D	To	LAT N	LON W	DEPTH	RMS	ERX	ERY	ERZ	Mag
881207	7 45 45.49	40N54.09	44E15.70	5.46	.52	1.41	.63	9.98	6.0

4. **Relocation of the early aftershocks with respect to the following master events:**

Date	Origin time	Lat	Long	Depth
* 31-12-1988	04h 07mn 09.45s	40°55.13'N	43°56.66'E	9.71
* 01-01-1989	22h 59mn 38.23s	40°46.76'N	44°22.93'E	3.13
* 03-01-1989	13h 48mn 47.10s	40°52.06'N	44°12.47'E	5.33
* 04-01-1989	07h 29mn 40.44s	40°53.32'N	44°14.96'E	4.94
* 05-01-1989	08h 15mn 13.64s	40°50.12'N	44°19.17'E	6.46
* 06-01-1989	07h 35mn 58.54s	40°53.85'N	43°56.67'E	4.92
* 08-01-1989	10h 26mn 47.71s	40°54.18'N	44°09.36'E	4.20

Y M D	To	LAT N	LON W	DEPTH	RMS	ERX	ERY	ERZ	Mag
881207	0806 26.39	40N50.83	44E00.64	4.89	0.61	0.37	0.24	09.10	4.9
881207	0857 03.49	40N53.59	44E01.65	4.20	0.44	0.22	0.18	10.00	3.0
881207	0928 37.49	40N48.36	44E22.85	6.34	0.48	0.40	0.34	08.55	3.0
881207	1020 26.94	40N55.06	44E05.69	5.33	0.69	0.61	0.28	09.39	3.0
881207	1056 50.39	40N52.99	44E12.82	6.34	0.61	0.21	0.16	02.11	4.2
881207	1101 04.07	40N56.21	44E08.73	6.34	0.96	0.20	0.20	02.37	3.9
881207	1103 32.24	40N54.79	44E09.76	4.20	0.53	0.16	0.14	10.00	3.9
881207	1209 26.46	40N53.10	44E13.16	4.20	0.42	0.20	0.17	10.00	3.8
881207	1212 55.96	40N54.51	44E02.50	4.20	0.90	0.21	0.16	10.00	3.0
881207	1223 06.63	40N51.62	44E12.70	4.20	1.00	0.39	0.35	10.00	3.0
881207	1230 45.13	40N53.59	44E11.96	5.33	0.32	0.27	0.70	09.98	3.0
881207	1247 58.33	40N54.13	44E08.05	6.34	0.56	0.43	0.29	08.35	3.0
881207	1404 39.23	40N55.30	44E00.78	4.20	0.58	0.27	0.25	10.00	3.0
881207	1410 14.46	40N56.40	44E13.01	6.34	0.83	0.66	0.30	08.19	4.3
881207	1437 14.16	40N48.88	44E24.29	6.34	0.60	0.22	0.15	01.76	4.0
881207	1446 29.28	40N52.03	44E14.34	5.46	0.43	0.22	0.16	03.13	3.0
881207	1503 00.87	40N53.80	44E12.22	5.46	0.78	0.23	0.21	09.41	3.0
881207	1554 52.73	40N53.25	43E58.67	5.46	0.90	0.33	0.22	08.33	3.0
881207	1647 48.19	40N56.26	44E03.54	4.89	0.53	0.14	0.18	05.47	3.0
881207	1650 02.36	40N55.34	44E02.80	4.20	0.80	0.46	0.35	10.00	3.0

Table 4. (*continued*)

Y M D	To	LAT N	LON W	DEPTH	RMS	ERX	ERY	ERZ	Mag
881207	1805 41.82	40N52.54	44E09.73	4.20	0.35	0.86	0.80	10.00	4.4
881207	1826 55.97	41N00.19	43E51.63	4.20	0.49	1.71	1.01	10.00	3.0
881207	1917 51.49	40N51.60	44E08.31	6.34	0.43	1.97	1.32	09.99	4.1
881207	2007 28.93	40N54.83	44E12.95	6.34	0.28	0.22	0.21	06.82	4.4
881207	2035 08.88	40N50.33	43E58.27	6.34	0.27	0.78	1.03	09.30	3.0
881207	2203 21.98	40N52.88	44E13.26	4.20	0.55	1.06	0.31	10.00	3.0
881207	2350 53.85	40N56.30	43E58.45	4.20	0.19	0.30	0.24	10.00	3.0
881208	0014 54.81	40N49.91	44E13.70	6.34	0.80	0.24	0.21	06.69	3.0
881208	0114 59.47	40N49.90	44E19.46	6.34	0.61	1.14	0.84	09.99	4.4
881208	0149 38.15	40N54.56	43E59.92	4.20	0.48	0.26	0.37	10.00	4.3
881208	0209 29.81	40N53.42	44E18.60	6.34	.15	1.54	1.33	09.99	4.2
881208	0604 50.37	40N57.08	44E04.87	5.46	0.87	2.85	1.86	09.36	4.0
881208	0746 00.43	40N46.51	44E24.57	6.34	0.55	0.23	0.14	02.21	4.6
881208	1014 14.72	40N48.55	44E19.79	6.34	0.43	0.59	0.55	07.21	4.3
881208	1246 54.43	40N53.40	43E57.19	4.20	0.27	1.83	2.22	10.00	4.1
881208	1441 36.28	40N55.90	44E11.44	6.34	0.54	0.18	0.17	06.10	3.0
881208	1759 15.76	40N51.80	44E10.86	6.34	0.64	0.96	1.41	08.93	4.2
881208	2032 05.78	40N53.42	44E11.81	6.34	0.43	0.19	0.16	02.05	4.5
881209	0112 13.34	40N52.45	44E12.66	3.13	0.44	0.16	0.17	09.99	3.0
881209	0450 27.89	40N45.27	44E21.96	5.33	0.32	0.15	0.14	04.21	3.0
881209	0831 07.15	40N54.38	44E08.92	6.34	0.38	0.14	0.15	02.14	3.0
881209	0854 26.09	40N50.27	44E11.44	6.34	0.06	0.42	0.49	07.91	3.0
881209	1401 25.62	40N54.49	44E08.42	6.34	0.45	0.24	0.17	02.72	4.1
881209	1413 57.21	40N54.97	44E02.00	4.20	0.26	0.19	0.16	10.00	3.0
881209	1423 01.21	40N51.72	44E18.06	5.46	0.30	0.20	0.16	02.39	3.0
881209	1448 23.60	40N55.63	44E07.86	4.20	0.74	0.74	0.54	10.00	3.0
881209	1516 15.00	40N51.71	44E13.54	5.46	0.26	0.19	0.35	05.33	3.0
881209	1916 33.35	40N47.32	44E21.83	5.46	0.50	0.23	0.18	04.22	4.1
881210	0000 46.28	40N44.52	44E23.03	5.33	0.29	0.35	0.43	08.83	3.0
881210	1913 57.76	40N48.92	44E18.61	5.46	0.35	0.14	0.18	07.03	4.2
881210	2125 02.74	40N57.11	44E04.53	3.13	0.32	0.49	0.32	09.99	3.0
881211	0355 10.90	40N51.70	44E13.60	5.46	0.95	0.16	0.18	03.13	4.4
881211	0458 11.56	41N 0.72	44E04.52	4.20	0.37	0.22	0.19	10.00	3.0
881211	0936 19.14	40N47.87	44E19.94	5.46	0.34	0.15	0.14	03.46	3.0
881211	1220 07.97	40N48.25	44E20.65	5.46	0.30	0.13	0.13	02.96	3.0
881211	2308 17.64	40N56.00	44E06.98	6.34	0.25	0.18	0.17	02.56	3.0
881212	0115 00.33	40N53.52	44E08.92	4.20	0.64	0.21	0.15	10.00	3.0
881212	0845 54.54	40N51.08	44E17.00	4.20	0.53	0.59	0.21	10.00	3.8
881212	1536 17.19	40N53.96	44E17.39	5.46	0.37	0.25	0.23	02.29	4.2
881212	1713 08.53	40N48.73	44E22.74	4.20	0.80	0.30	0.15	10.00	3.0
881212	1722 33.27	40N54.02	44E03.43	3.13	0.59	0.21	0.14	09.99	3.6
881212	1803 41.89	40N44.78	44E21.07	4.89	0.16	0.26	0.24	08.59	3.0
881213	0421 37.33	40N54.58	44E13.18	6.34	0.45	0.17	0.17	01.74	4.1
881213	1112 36.39	40N54.22	44E01.01	4.20	0.41	0.27	0.19	10.00	3.2
881213	2135 21.73	40N55.29	44E05.87	3.13	0.69	0.19	0.16	09.99	3.5
881214	2049 08.76	40N52.98	44E09.28	4.20	0.44	0.17	0.15	10.00	3.9
881215	0414 08.89	40N46.89	44E21.66	4.20	0.29	0.35	0.13	10.00	3.2
881215	1543 44.74	40N53.74	43E59.00	4.89	0.17	0.22	0.18	07.55	4.5
881216	1853 02.58	40N53.70	44E05.54	4.20	0.80	0.18	0.22	10.00	4.3
881217	2333 18.08	40N53.38	44E09.09	5.33	0.08	0.26	0.20	04.14	3.3
881218	0408 52.66	40N44.69	44E22.62	6.34	0.33	0.18	0.26	04.82	3.3
881218	1307 02.19	40N57.34	44E03.55	4.20	0.94	0.25	0.17	10.00	3.0
881218	1749 33.39	40N51.01	44E12.09	6.34	0.66	0.31	0.61	09.07	3.6
881218	1952 06.00	40N56.22	44E02.76	4.20	0.22	0.23	0.19	10.00	3.3
881218	2000 39.47	40N48.92	44E17.30	6.34	0.58	0.21	0.41	07.52	3.3
881220	0004 54.09	40N47.31	44E25.28	5.46	0.74	2.03	0.78	10.00	4.5

Solutions with RMS > 1 s were disregarded in all cases. An overall comparison between the two methods for the 40 common events shows that 90 per cent of them do not differ by more than 5 km. Based on this result, we trust the epicentre locations from the regional permanent network with station corrections to be accurate within 5 km. In the following, we present only the results obtained by the second method (master events) since this sequence is more complete.

The main shock was preceded by a foreshock of magnitude $M_L = 3$ on December 6 at 15 hr 27 min, namely 16 hr 14 min before. We located this foreshock relative to the main shock by using arrival times from seven common stations. Its epicentre lies at about 8 km to the southwest of the main shock and slightly outside the aftershock cloud. Nevertheless this location is not well constrained since the RMS value is of 0.9 s.

The main shock was relocated by the second method at 40.886°N, 44.261°E, less than 3 km from the Obninsk determination which includes arrival times from regional and distant stations. The epicentre relocated by the first method, using station delays from 17 regional stations, is
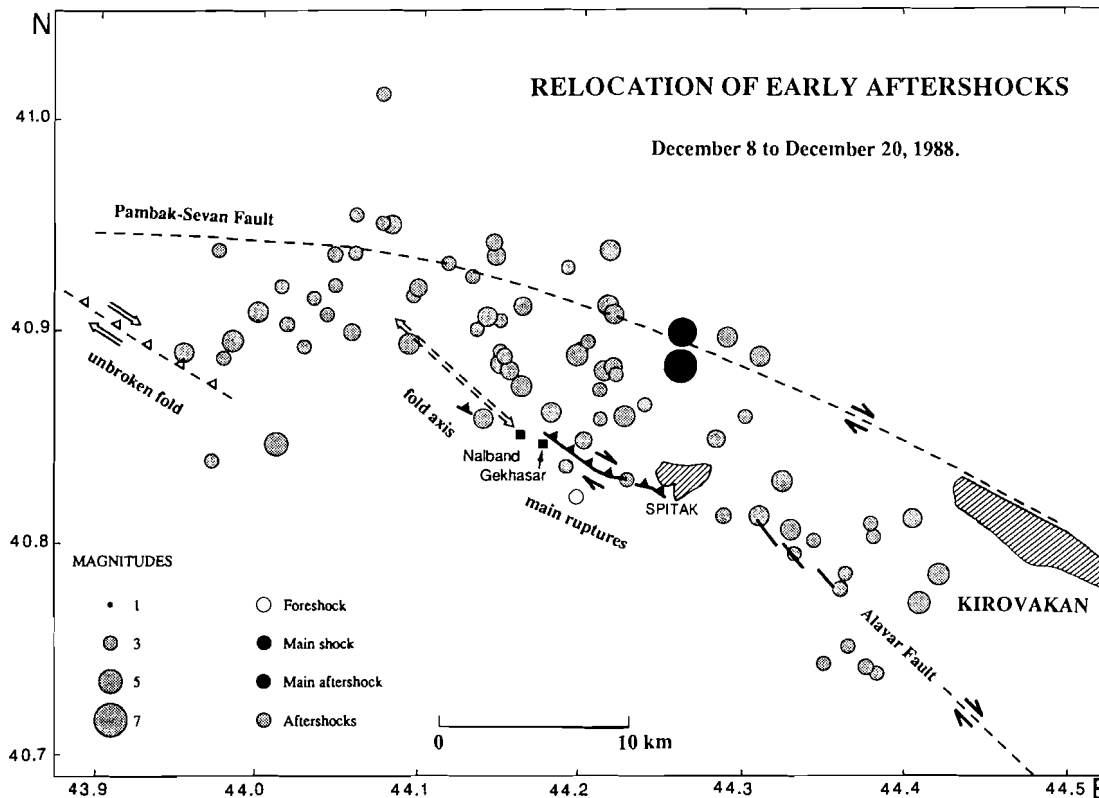
N

41.0

RELOCATION OF EARLY AFTERSHOCKS

December 8 to December 20, 1988.

Pambak-Sevan Fault

40.9

unbroken fold

fold axis

Nalband
Gekhasar

main ruptures

SPITAK

KIROVAKAN

Alavar Fault

40.8

MAGNITUDES

- 1   ○ Foreshock
⊙ 3   ● Main shock
⊚ 5   ● Main aftershock
⊛ 7   ⊙ Aftershocks

0   10 km

40.7

43.9   44.0   44.1   44.2   44.3   44.4   44.5 **E**

Figure 8. Map of epicentral relocations (Table 4) from the data of the permanent network of stations of Fig. 7, from 1988 December 6 to 1988 December 24.

found to be at 40.881°N, 44.265°E, so our two independent determinations differ by 650 m only.

Careful examination of broad-band waves from distant records shows that the main energy burst was preceded by a small signal (foreshock) a few seconds before (Haessler et al. 1991). It was impossible to identify the initial time of the large amplitudes on the records of the Armenian stations, thus the relocated epicentre corresponds to the weak initial phase. However Kondorskaya (personal communication) performed a relative location of these two events (the arrival time of the first small phase with respect to the arrival of the large amplitudes) by using records at teleseismic distances and found that they are at the same place within error bars, and thus the epicentre of the main shock has the position we computed with an accuracy probably better than 3 km. These considerations confirm the place of initiation of the main shock to be just a few kilometres north of Spitak, at the eastern edge of the central segment and near the intersection with the northern extension of the Alavar fault

The strongest aftershock [4 min 20 s after the main shock, 40.974°N, 44.246°E, $m_b = 5.9$ (NEIC); 40.80°N, 44.16°E, $m_b = 6.0$ (Obninsk)] caused extensive damage to buildings already weakened by the main earthquake and numerous casualties. Unfortunately, it was not possible to read the P-wave onset at more than four Armenian stations: BAW, LEN, ERE and ARR. Differences of P arrival times relative to those of the main shock are the same at all of the stations (within 0.2 s) but the BKR bulletin indicates that this difference is 1.2 s smaller. We verified that the epicentre is

close to the one of the main shock, and slightly to the north by computing its position relative to the main shock (Fig. 8). Although this location is weakly constrained we do not believe that the error is more than 15 km. We may ask whether this strong aftershock was responsible for the rupture of the southeastern segment. The latter argument suggests that the aftershock did not take place on that part of the southeastern segment as we postulated in a previous paper (Cisternas et al., 1989). And another piece of information, the modelling of broad-band seismograms (Haessler et al. 1991), also implies that the Alavar segment very likely ruputed a few seconds after the intial shock and not at the time of the strong aftershock.

No other aftershock of the Spitak earthquake exceeded the magnitude $M_L = 5.0$. The epicentres (Fig. 8) exhibit the same overall pattern already seen on Fig. 3, but with more dispersion. A large number (40 per cent) of the located aftershocks occurred during the first 24 hr after the main shock. Nevertheless, not all of the aftershocks could be adequately located during the first day due to the high density of events and the consequent inference of the recordings, and some of the early aftershocks may be absent from Fig. 8.

We do not observe any evident clustering in time or space. Therefore, as we pointed out above, the whole aftershock zone of Fig. 8 was active after the main shock, in agreement with the broad-band modelling that shows that the five segments ruptured all along within about 15 s (Haessler et al. 1991).

CONCLUSIONS

Aftershocks of the Spitak earthquake have been recorded by a dense network of 26 portable seismic stations, thus providing a detailed observation of the aftershock sequence with high-quality numerical records.

Focal mechanisms of aftershocks and their space distribution, together with the mapping of surface ruptures and observations of deformation of active folds (Philip *et al.* 1991), led us to propose a five segment fault model of the main earthquake (Fig. 3). Two of them break up the surface, namely the Alavar (N140°) and the Spital–Gekhasar (N120°) segments. Two other segments are hidden under 'en échelon' blind folds west of Ghekhasar. The fifth segment is located to the northwest of the aftershock zone, and begins near the surface trace of the Pambak–Sevan fault. Maximum depths are very shallow (6 km) along the Alavar segment but they increase towards the west, reaching more than 15 km under the western and northwestern segments. The seismic moment of the Alavar segment is 1/6 of the total moment.

The set of polarity data from the first arrivals of the aftershocks is in agreement with a single stress tensor which is compatible with the northward motion of the Arabian plate. The focal mechanisms are well constrained, either when calculated individually by two independent methods, or when obtained at the same time as the stress tensor in a maximum likelihood procedure, the likelihood being 97 per cent in this latter case. The σ_1 axis is horizontal, oriented N344°, and the stress regime corresponds to triaxial compression. Right lateral strike–slip on an almost vertical plane dominates in the Alavar and the northwestern segment, while reverse motion with a smaller right lateral component on a surface dipping 50° to the NE, is typical of the Spitak–Gekhasar segment and of the blind folds.

The general aspect of the relocated events, corresponding to the period going from the occurrence of the main shock to the installation of the portable network, is very similar but less precise than that of the well-located aftershocks. The relocation of the main shock gives an epicentre at 40.886°N and 44.261°E a few kilometres to the north of Spitak. The relative locations of the foreshock, the main shock, and the strongest aftershock, place these three events near the intersection between the Alavar fault and the Pambak–Sevan fault. The implication is that the Spitak fault differs from the Alavar and Pambak–Sevan faults near the surface, but it is strongly related to them at depth, smoothing the sharp bend formed by the intersection of these two main tectonic features.

The above results make part of a comprehensive study that includes neotectonics, near-field local seismic stations and teleseismic broad-band recordings, geodynamic models of the region, deformation associated with the earthquake and palaeoseismology, thus permitting a global view of the geometry and time evolution of the source process (Philip *et al.* 1991; Haessler *et al.* 1991). The mechanism of the main shock and those of the aftershocks are in agreement with the stress regime previously obtained from a general study of the recent tectonics of the Caucasus. The fault activated by this earthquake is not easily recognized in satellite images, and appears as a secondary feature related to well-defined main accidents such as the Pambak–Sevan and Alavar faults. Nevertheless, it gives precise complementary information about the recent tectonics of the southern border of the Lesser Caucasus, a region where approximately EW oriented reverse faulting and folding coexists with NS volcanic alignments and diagonal strike–slip faulting.

REFERENCES

Aki, K. & Richards, P. G., 1980. *Quantitative Seismology: Theory and Methods*, Vol. 1, Freeman, San Francisco.

Besse, P., 1986. Relocalisation relative d'événements sismiques, appliqué à la région Sud du Lac Ghoubbet situé dans la République de Djibouti, *Rapport DEA*, Université Paris VII.

Cisternas, A. *et al.*, 1989. The Spitak (Armenia) earthquake of 7 December 1988: field observations, seismology and tectonics, *Nature*, **339**, 675–679.

Dewey, J. W., 1972. Seismicity and tectonics of Western Venezuela, *Bull. seism. Soc. Am.*, **62**, 1711–1751.

Dufumier, H., 1989. Détermination de mécanismes au foyer à partir d'enregistrement d'ondes de volume et de surface, *Diplome d'Ingénieur Géophysicien*, Université L. Pasteur, Strasbourg.

Haessler, H., Deschamps, A., Dufumier, H., Fuenzalida, H. & Cisternas, A., 1991. The rupture process of the Armenian earthquake from broad-band teleseismic body wave records, *Geophys. J. Int.*, submitted.

Jimenez, E., Cara, M. & Rouland, D., 1989. Focal mechanism of moderate size earthquakes from the analysis of single station three components surface wave records, *Bull. seism. Soc. Am.*, **79**, 955–972.

King, G. & Yielding, G., 1984. The evolution of a thrust fault system: processes of rupture initiation, propagation and termination in the 1980 El Asnam (Algeria) earthquake, *Geophys. J. R. astr. Soc.*, **77**, 915–933.

Klein, F.. W., 1978. Hypocenter location program HYPO-INVERSE, *Open-File Rept 78-694*, US Geological Survey, Boulder, CO.

Lyon-Caen, H. *et al.*, 1988. The 1986 Kalamata (South Peloponnesus) earthquake: detailed study of a normal fault, evidences for east–west extension in the Hellenic Arc, *J. geophys. Res.*, **93**, **B12**, 14 967–15 000.

Pacheco, J. F., Estabrook, C. H., Simpson, D. W. & Nabelek, J. L., 1989. Teleseismic body wave analysis of the 1988 Armenian earthquake, *Geophys. Res. Lett.*, **16**, 1425–1428.

Philip, H., Cisternas, A., Gvishiani, A. & Gorshkov, A., 1989. The Caucasus: an actual example of the initial stage of continental collision, *Tectonophysics*, **161**, 1–21.

Philip, H., Rogozhin, E., Cisternas, A., Bousquet, J. C., Borisov, B. & Karakhanian, A., 1991. The Armenian earthquake of

1988 December 7: faulting and folding, neotectonics and palaeoseismicity, *Geophys. J. Int.*, submitted.

Rivera, L. & Cisternas, A., 1990. Stress tensor and fault plane solutions for a population of earthquakes, *Bull. seism. Soc. Am.*, **80**, 600–614.

Scholz, C. H., 1990. *The Mechanics of Earthquakes and Faulting*, Cambridge University Press, Cambridge, UK.

Stein, R. & King, G. C., 1984. Seismic potential revealed by surface folding: 1983 Coalinga, California earthquake, *Science*, **224**, 869–872.

Tarantola, A. & Valette, B., 1982. Generalized nonlinear inverse problems solved using the least-squares criterium, *Rev. Geophys. Space Phys.*, **20**, 219–232.

Udías, A., Buforn, E., Brillinger, D. & Bolt, B., 1982. Joint statistical determination of fault-plane parameters, *Phys. Earth planet. Inter.*, **30**, 178–184.